Theoretical Notes
Note 241

UNCLASSIFIED
SECURITY CLASSIFICATION OF THIS PAGE (*When Data Entered*)

REPORT DOCUMENTATION PAGE

READ INSTRUCTIONS BEFORE COMPLETING FORM

1. REPORT NUMBER
HDL-TR-1725

2. GOVT ACCESSION NO.

3. RECIPIENT'S CATALOG NUMBER

4. TITLE (*and Subtitle*)
Transient Ionization Effects from
Primary Gamma Fission Radiation
in the Upper Atmosphere

5. TYPE OF REPORT & PERIOD COVERED
Technical Report

6. PERFORMING ORG. REPORT NUMBER

7. AUTHOR(*s*)
John P. Roberts
John S. Wicklund

8. CONTRACT OR GRANT NUMBER(*s*)
DA: 1W162118AD51

9. PERFORMING ORGANIZATION NAME AND ADDRESS
Harry Diamond Laboratories
2800 Powder Mill Road
Adelphi, MD 20783

10. PROGRAM ELEMENT, PROJECT, TASK AREA & WORK UNIT NUMBERS
Program Element:
6.21.18.A

11. CONTROLLING OFFICE NAME AND ADDRESS
Commander
US Army Materiel Command
Alexandria, VA 22333

12. REPORT DATE
October 1975

13. NUMBER OF PAGES
53

14. MONITORING AGENCY NAME & ADDRESS(*If different from Controlling Office*)

15. SECURITY CLASS. (*of this report*)
Unclassified

15a. DECLASSIFICATION/DOWNGRADING SCHEDULE

16. DISTRIBUTION STATEMENT (*of this Report*)

Approved for public release; distribution unlimited.

17. DISTRIBUTION STATEMENT (*of the abstract entered in Block 20, if different from Report*)

18. SUPPLEMENTARY NOTES

HDL Project No.: X51423
AMCMS Code: 612118.11.D5100

19. KEY WORDS (*Continue on reverse side if necessary and identify by block number*)

Gamma
Photon
Transport
Ionization

20. ABSTRACT (*Continue on reverse side if necessary and identify by block number*)

Gamma-radiation transport at deep penetration distances in the atmosphere has been studied as a function of time for a fission gamma unit-impulse source at a 45-km altitude. The Monte Carlo calculation included altitude-dependent air density, curvature of the earth, and Rayleigh scattering and polarization of the photons. Data were obtained on energy, angle, and time distributions for 20 detector positions.

The results show a large contribution to Compton ionization production rates at late (~10 to 100 μs) local times due to the arrival of multiply scattered gamma rays. Maintaining an energy cutoff as low as 10 keV has shown a pronounced effect on the total ionization at some detector locations. The results cast some doubt on the validity of previous calculations of gamma-induced atmospheric EMP.

CONTENTS

APPENDICES

FIGURES

TABLES

1. INTRODUCTION

The authors have calculated radiation transport for primary gamma and neutron sources to determine electromagnetic-pulse (EMP) source drivers-ionization production rates due to primary and secondary gamma photons and Compton source currents. The FASTER III Monte Carlo code[1] was modified considerably to provide the required data. Photon cross-section data were taken from Oak Ridge National Laboratory Radiation Shielding Information Center data tape DLC-17. Incoherent and coherent scattering form factor values were obtained from work by Veigele and coworkers.[2] Standard atmosphere data are included in the FASTER III code.[1] The values determined in these calculations will be used by the Electromagnetic Effects Laboratory of HDL in future EMP code calculations as source data. Preliminary results of this work were first presented at a Defense Nuclear Agency (DNA) EMP technical meeting in February 1974.[3] In addition, later work was presented at the American Nuclear Society Winter Meeting in October 1974.[4]

The results in this study are from a primary gamma source (an unclassified fission gamma spectrum[5]) at 45 km above the earth. (Above 50 km, the x-ray source term for EMP may predominate.[6]) Point detectors are located along radials from the source at distances corresponding to 1, 5, 10, 15, and 20 mean free path (mfp) lengths for a 14-MeV neutron (fig. 1). (This unit of measure was chosen to simplify comparison between primary gamma and neutron-secondary gamma-induced ionization.

---

[1] *T. M. Jordan, FASTER III, A Generalized Monte Carlo Computer Program for the Transport of Neutrons and Gamma Rays, vol. II, Users Manual, ART Research Corporation, ART-45 (November 1970).*

[2] *W. J. Veigele et al, X-Ray Cross Section Compilation from 0.1 keV to 1 MeV, Input Data and Supplemental Results, vol. II, Revision 1, Defense Nuclear Agency Report 2433F (31 July 1971).*

[3] *J. P. Roberts and J. S. Wicklund, Late-Time EMP Source Calculations at 45-km Height of Burst, Minutes of the EMP Phenomenology Meeting at Science Applications, Inc., La Jolla, CA, 12-13 February 1974, Report SAI-74-211-LJ (25 March 1974), 83-86.*

[4] *J. P. Roberts and J. S. Wicklund, Gamma-Induced Ionization Rate Pulse Broadening in the Upper Atmosphere, ANS Transactions, 19 (October 1974), 441-442.*

[5] *W. E. Selph and M. B. Wells, Weapons Shielding Handbook (U), DASA 1892-4 (December 1969). (SECRET--RESTRICTED DATA)*

[6] *D. F. Higgins, C. L. Longmire, and A. A. O'Dell, A Method for Estimating the X-Ray Produced Electromagnetic Pulse Observed in the Source Region of a High-Altitude Burst (DNA-3218T), Mission Research Corporation (29 November 1973).*

The neutron data are reported separately.[7] The position of the lowest detector directly below the source (at 20 mfp lengths) is 9.75-km aboveground. This is close to that region of the atmosphere in which mass equivalent range scaling is feasible for calculated results.[8] The radials along which the detectors are positioned are at 5, 30, 60, and 90 deg below the horizontal. Most detectors along the 5-deg radial lie off the horizontal scale of the plot (not shown in fig. 1).

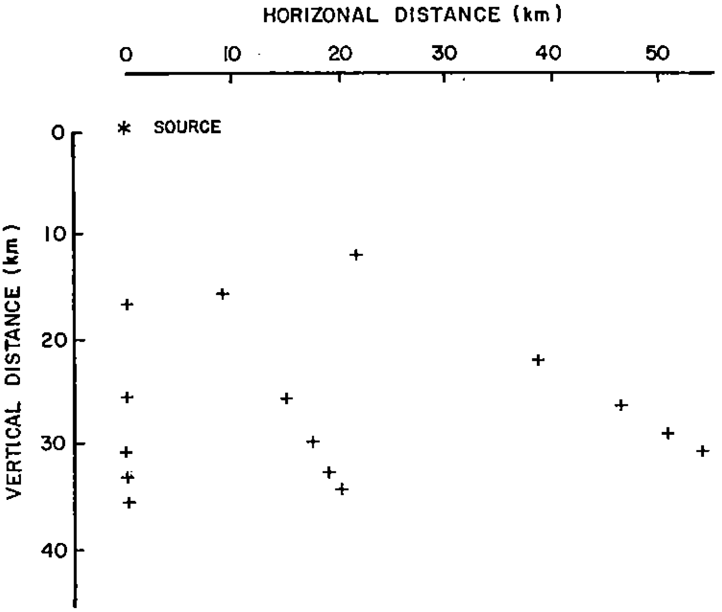

Figure 1. Source detector geometry.

The number of Monte Carlo histories for each detector was selected as a compromise between computer time and reasonable (~10 percent) standard deviations in the time bins, varying between 22,000 and 68,000 histories. For most detectors, 25,000 histories proved sufficient.

---

[7] *J. P. Roberts and J. S. Wicklund, Transient Ionization Effects from Neutron-Secondary Gamma Radiation in the Upper Atmosphere, Harry Diamond Laboratories TR-1727 (October 1975).*

[8] *E. A. Straker, Status of Neutron Transport in the Atmosphere, ORNL-TM-3065 (29 July 1970).*

2. RESULTS

The results from the 20 detector positions are shown in figures 2 to 21. Ionization production rate in megaelectronvolts per cubic meter-second is plotted as a function of local time in seconds. Local time commences with arrival of the first unscattered gamma ray at the detector position. The initial time bin for each detector includes the unscattered component, but it is not discussed here because it depends strongly on the time history of the source.

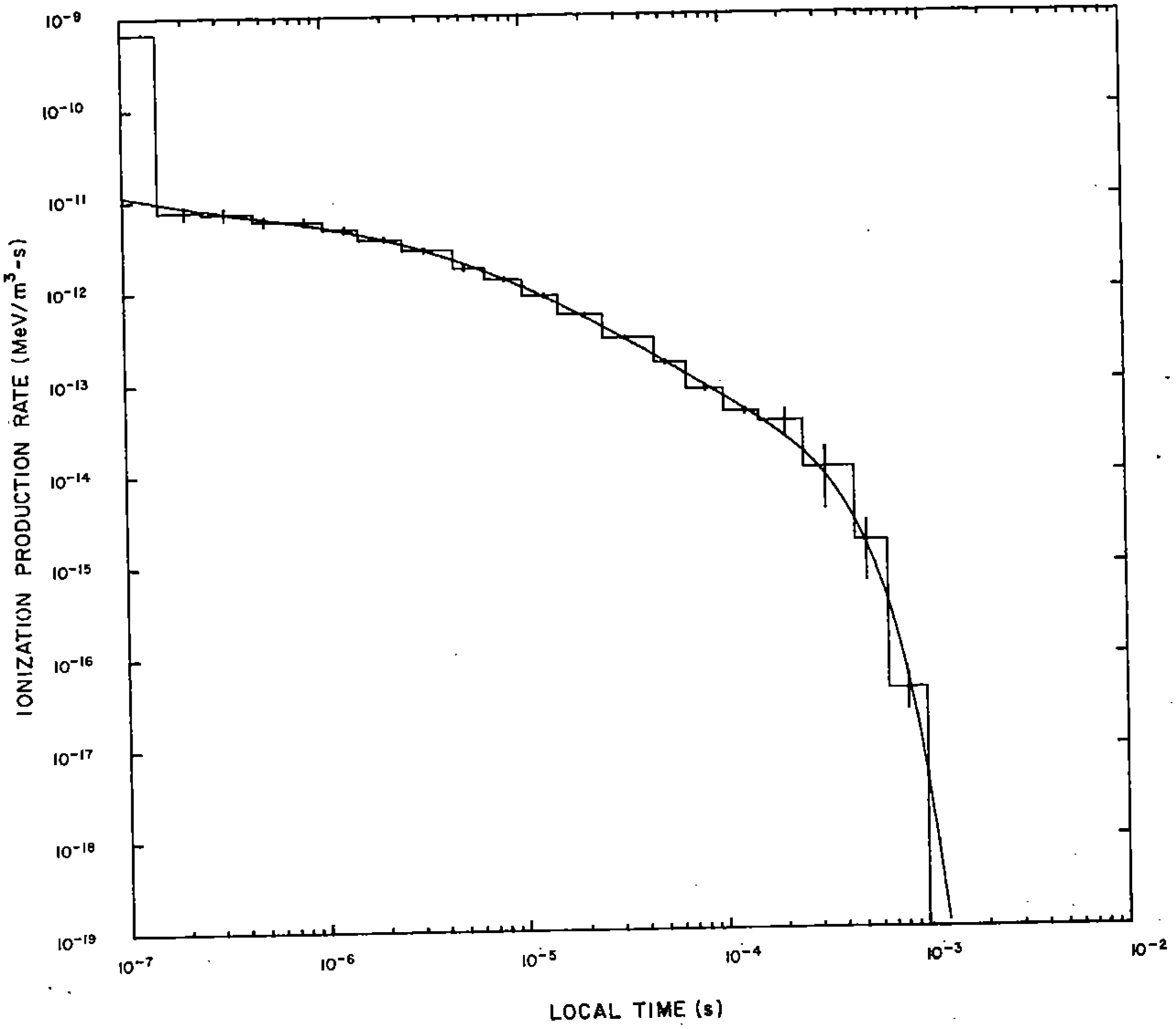

Figure 2. Ionization rate versus time for detector 1.

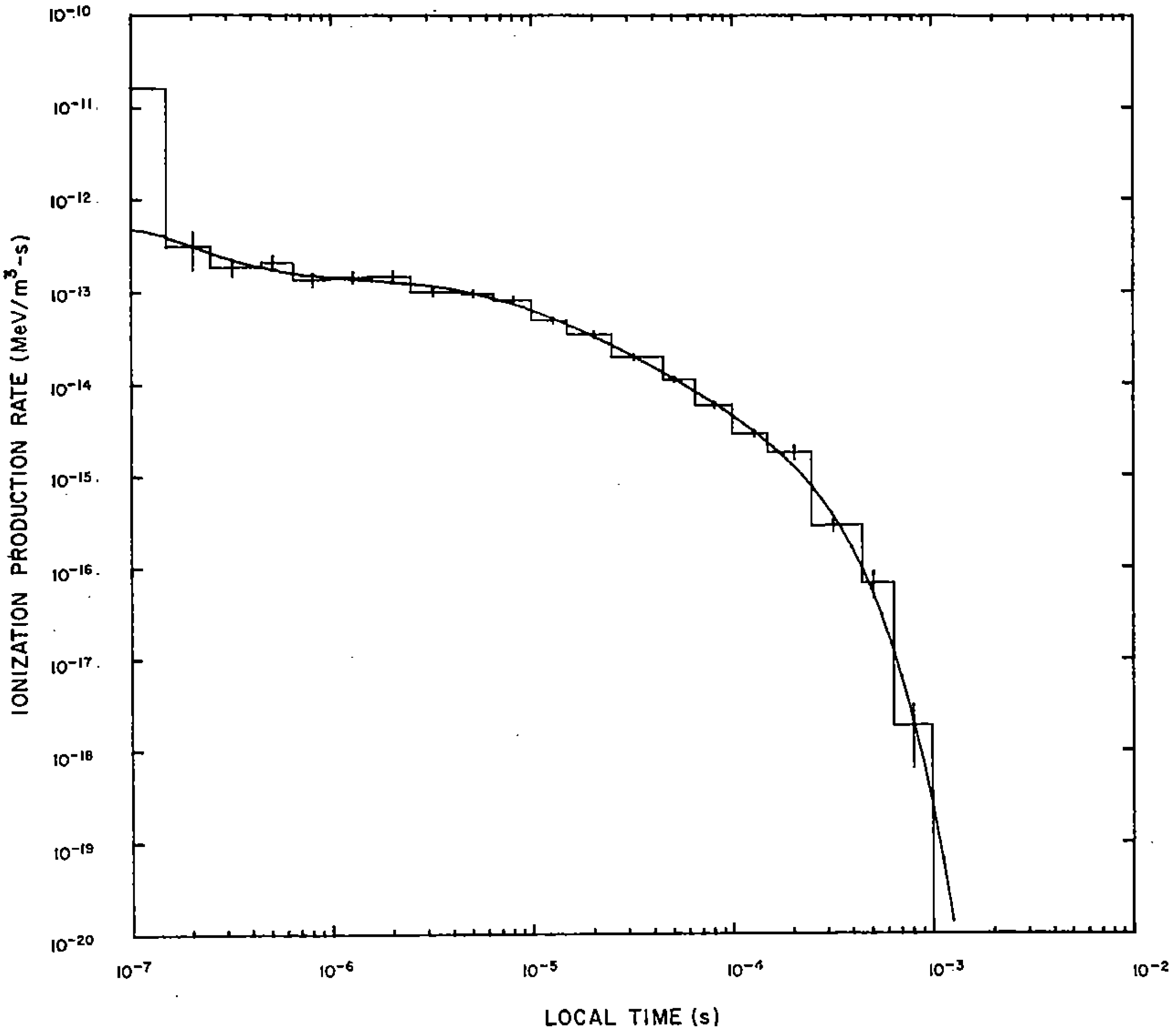

Figure 3. Ionization rate versus time for detector 2.

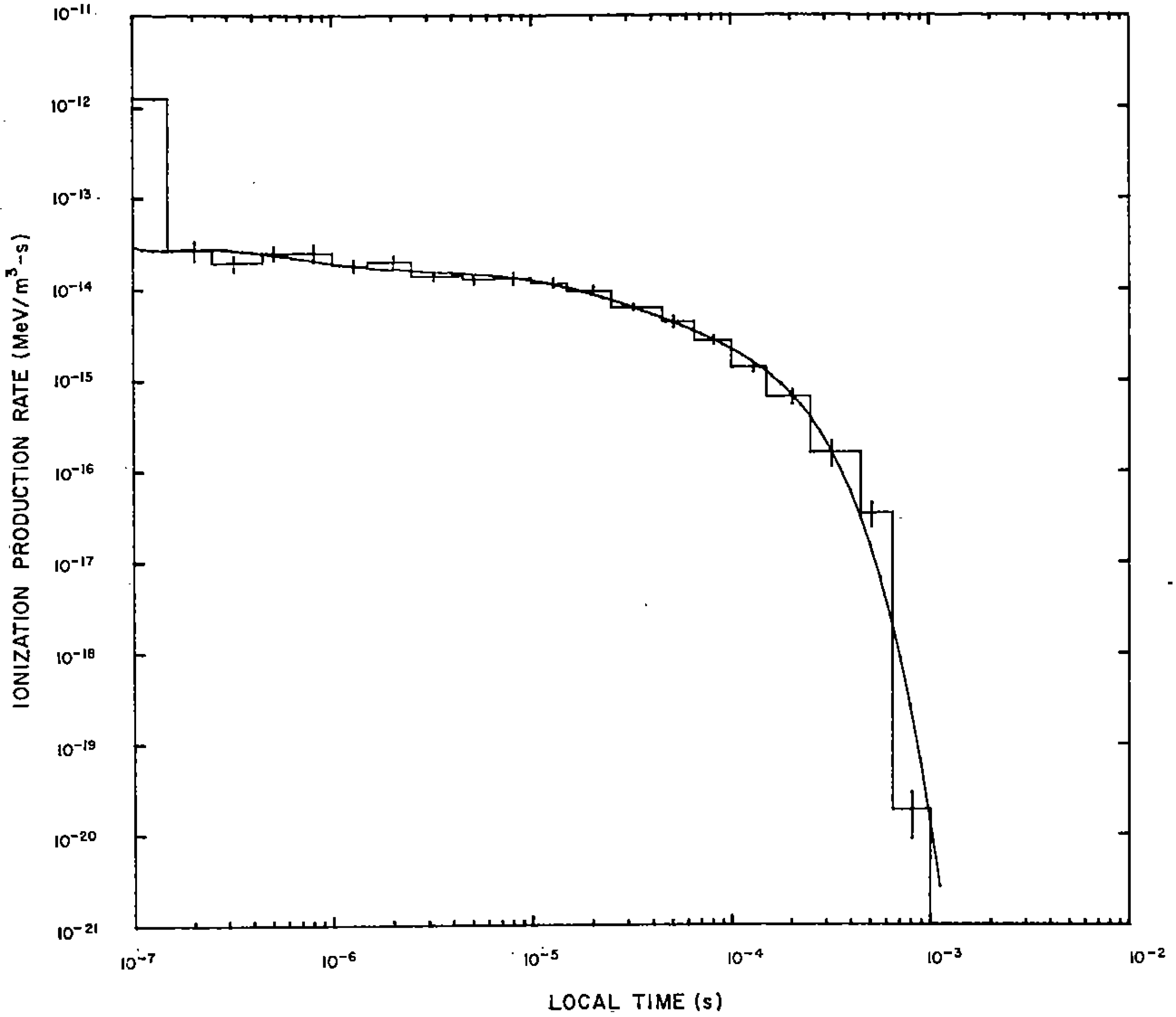

Figure 4. Ionization rate versus time for detector 3.

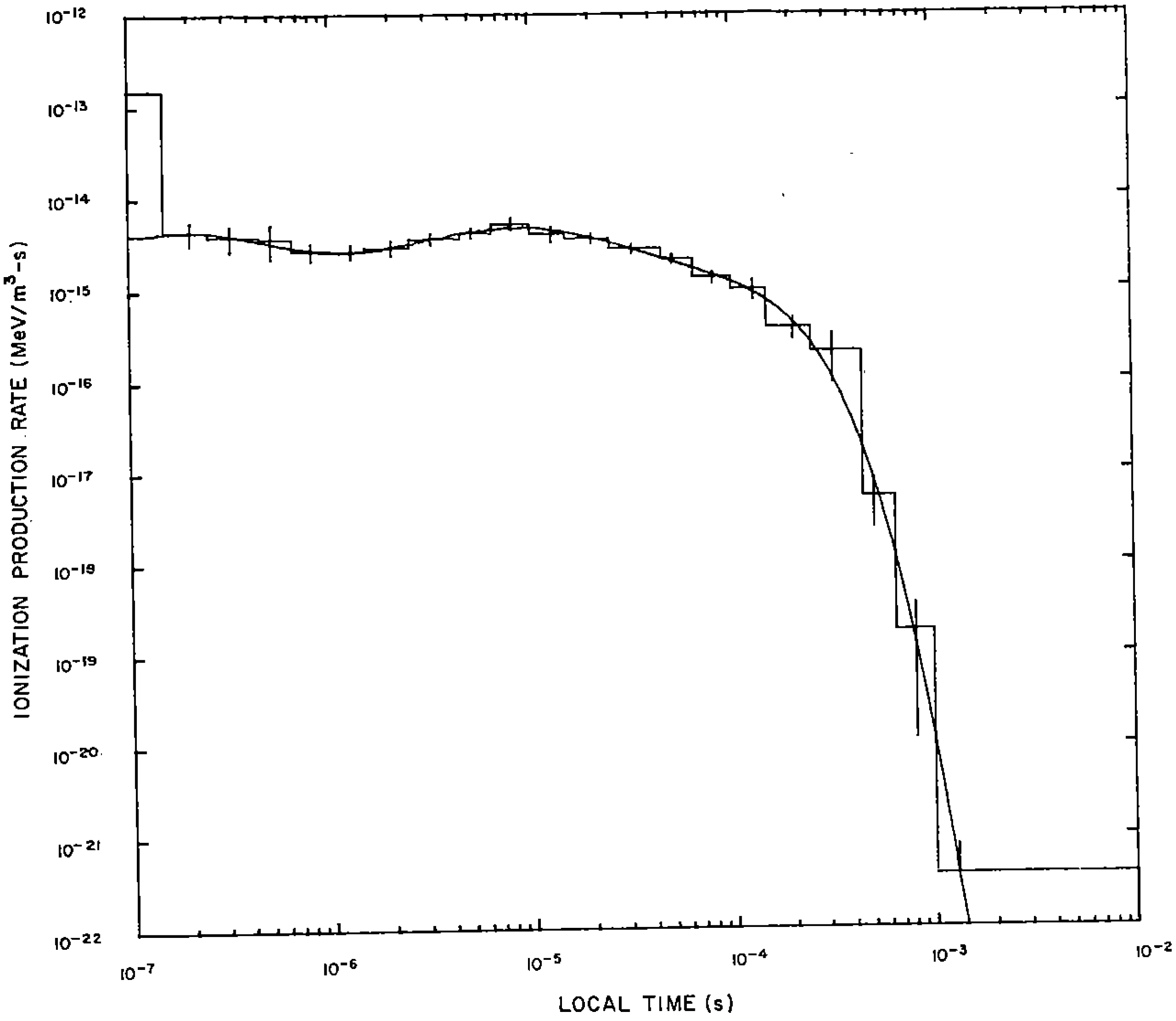

Figure 5. Ionization rate versus time for detector 4.

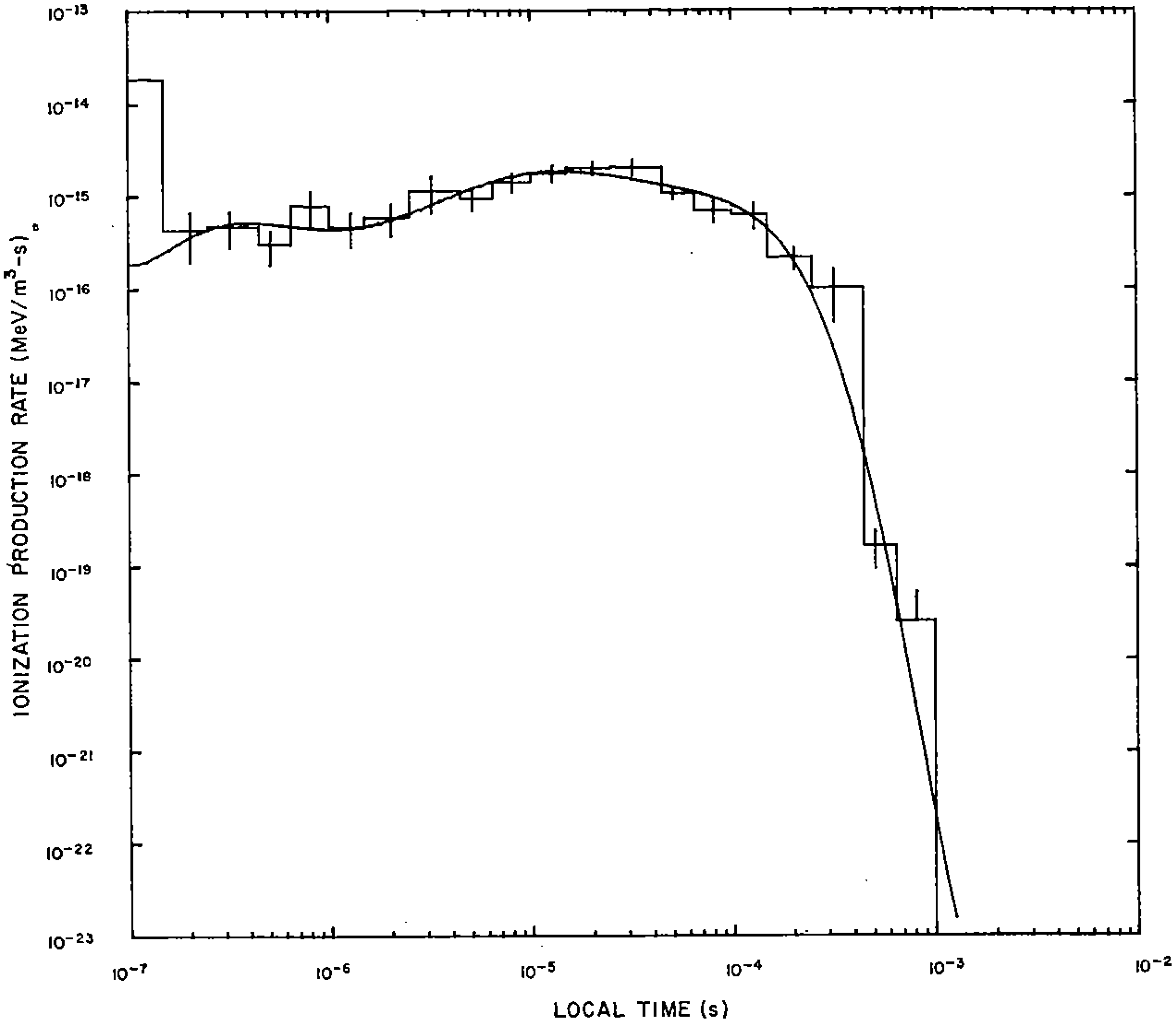

Figure 6. Ionization rate versus time for detector 5.

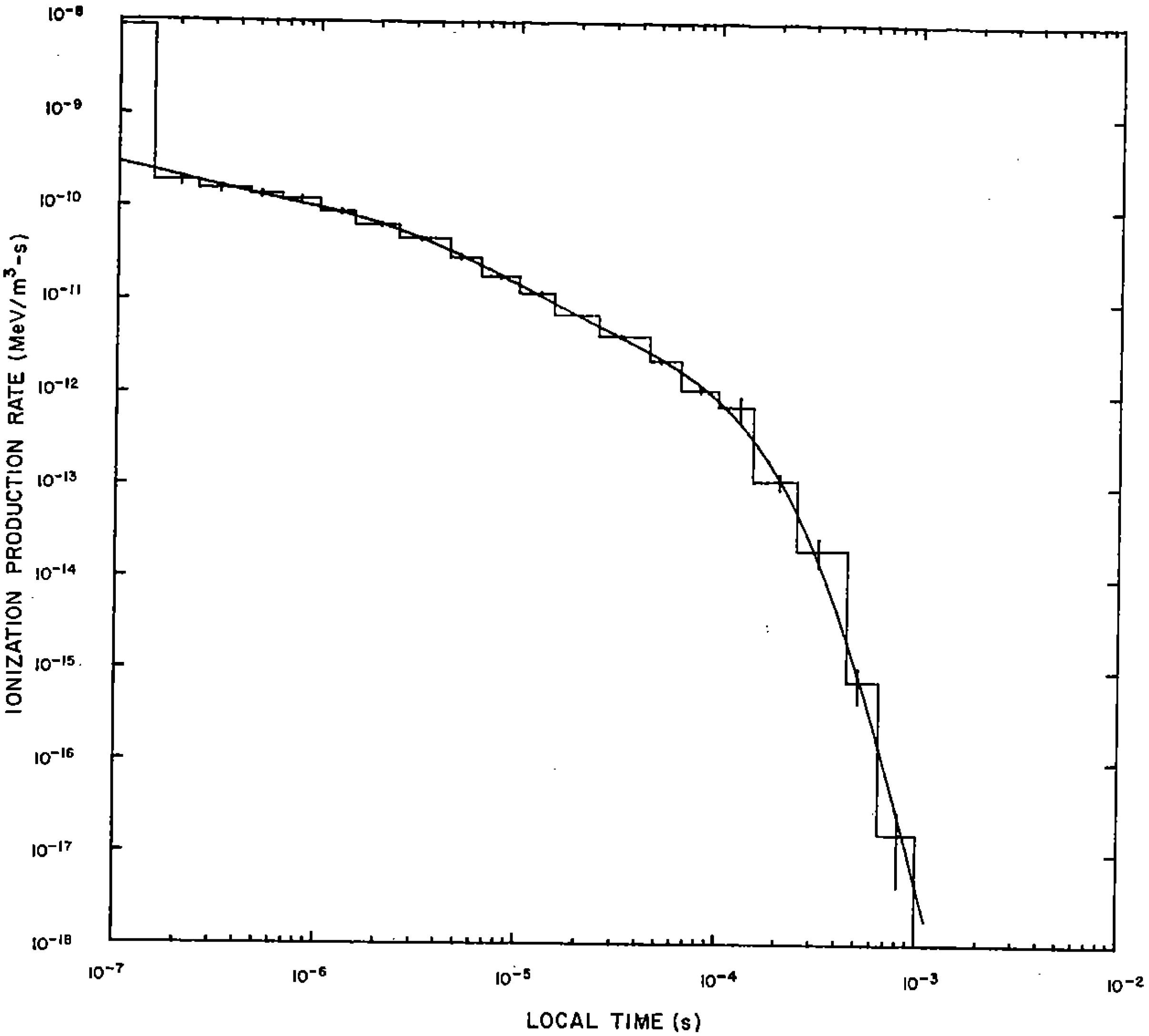

Figure 7. Ionization rate versus time for detector 6.

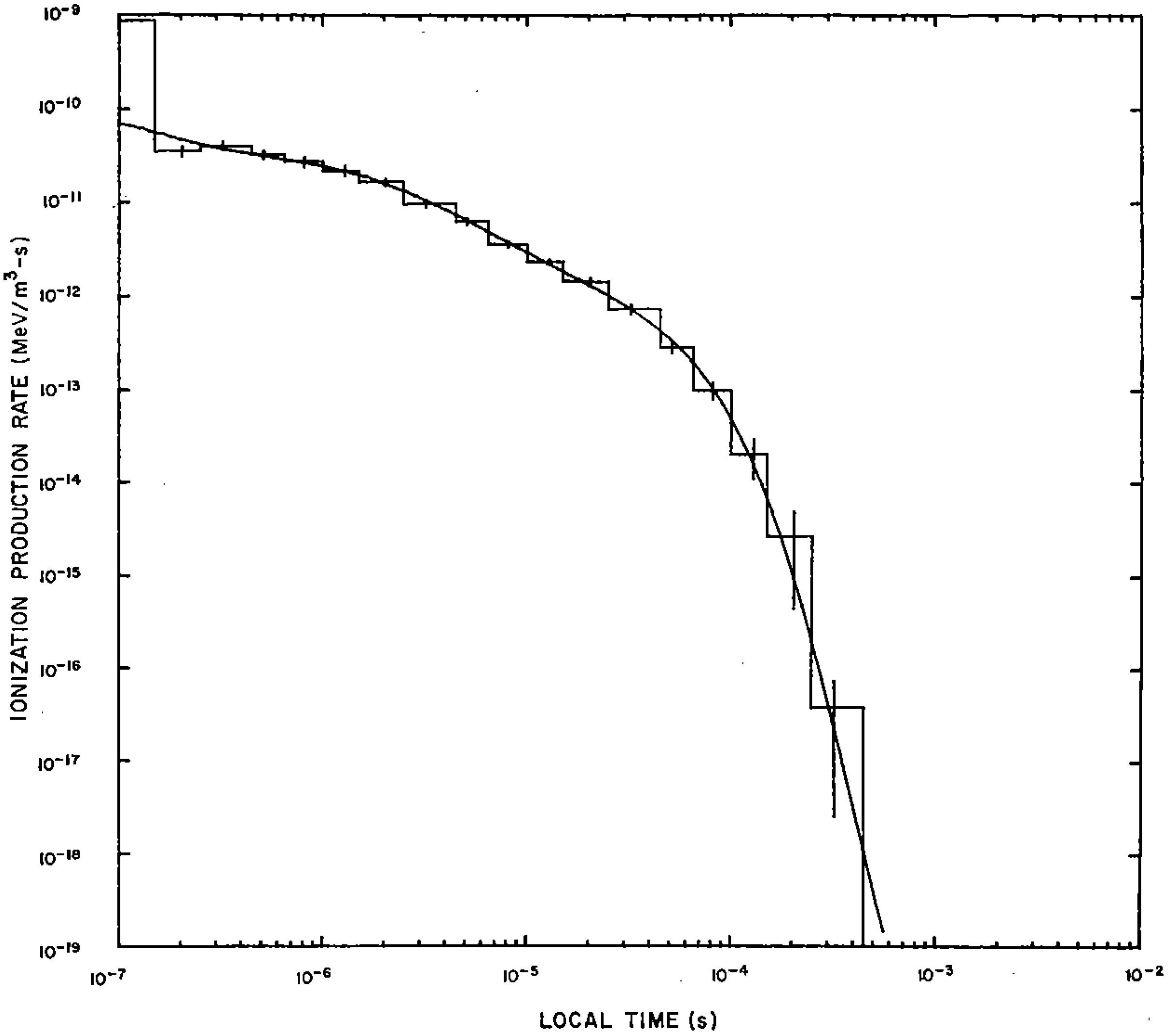

Figure 8. Ionization rate versus time for detector 7.

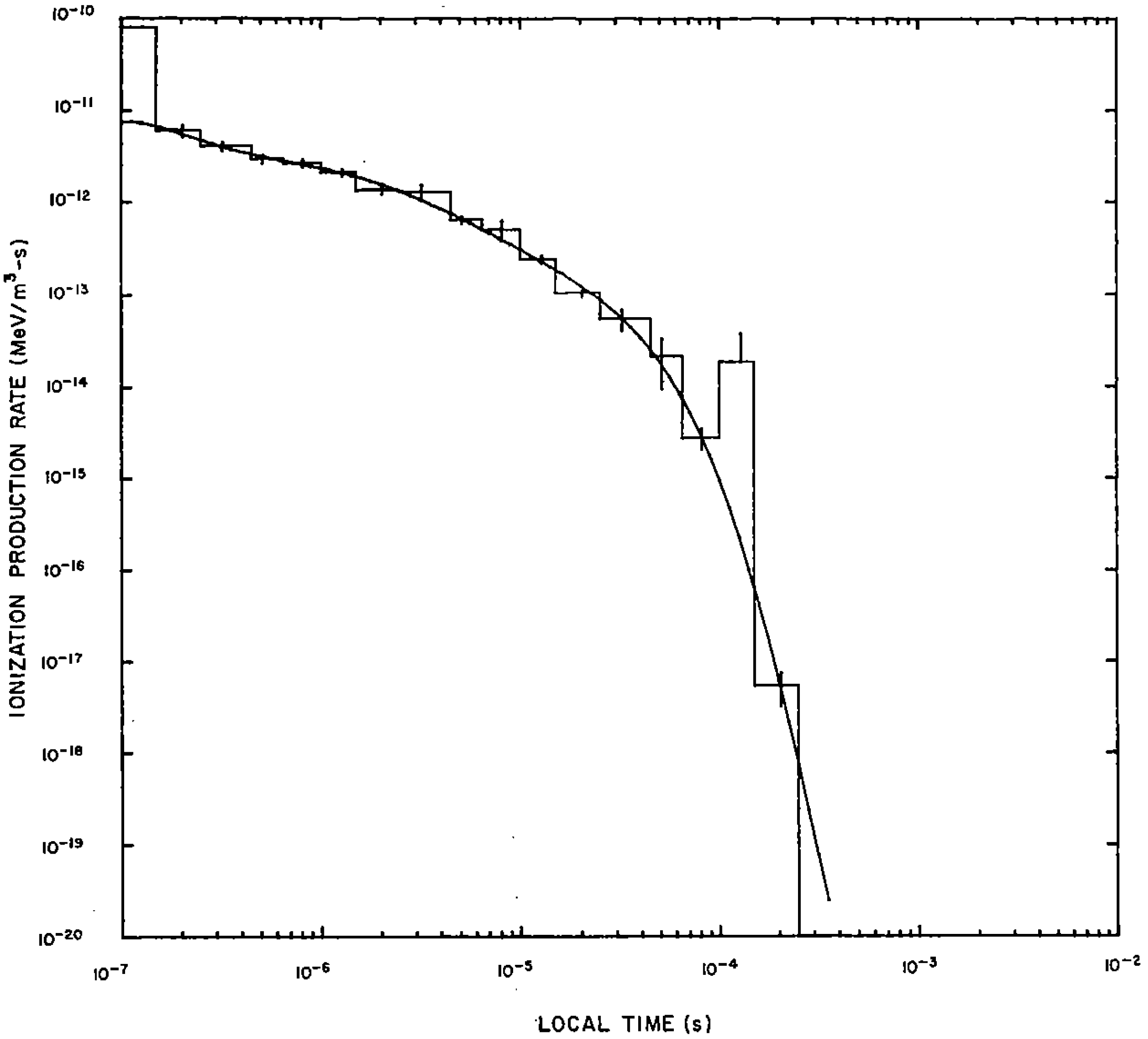

Figure 9. Ionization rate versus time for detector 8.

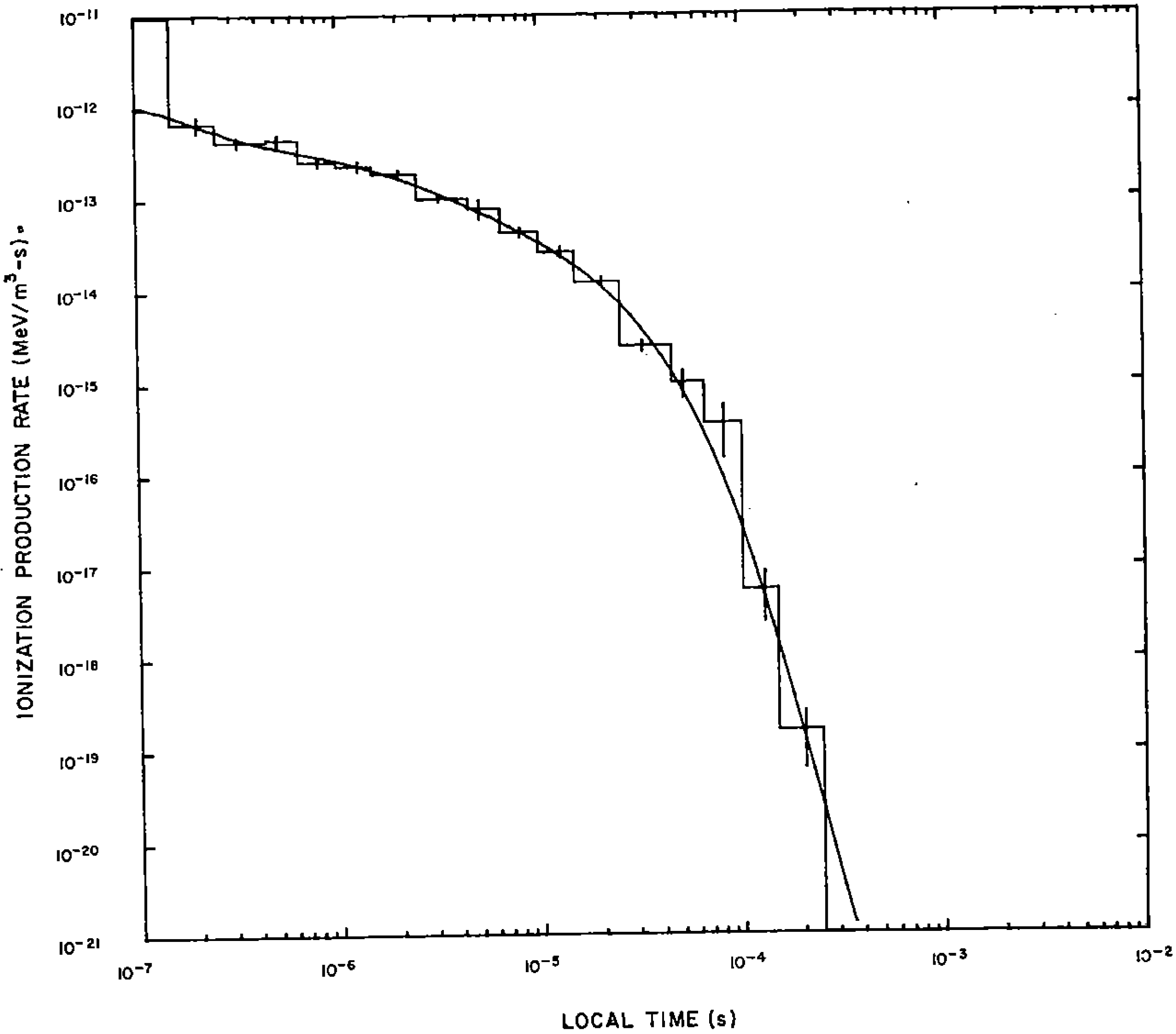

Figure 10. Ionization rate versus time for detector 9.

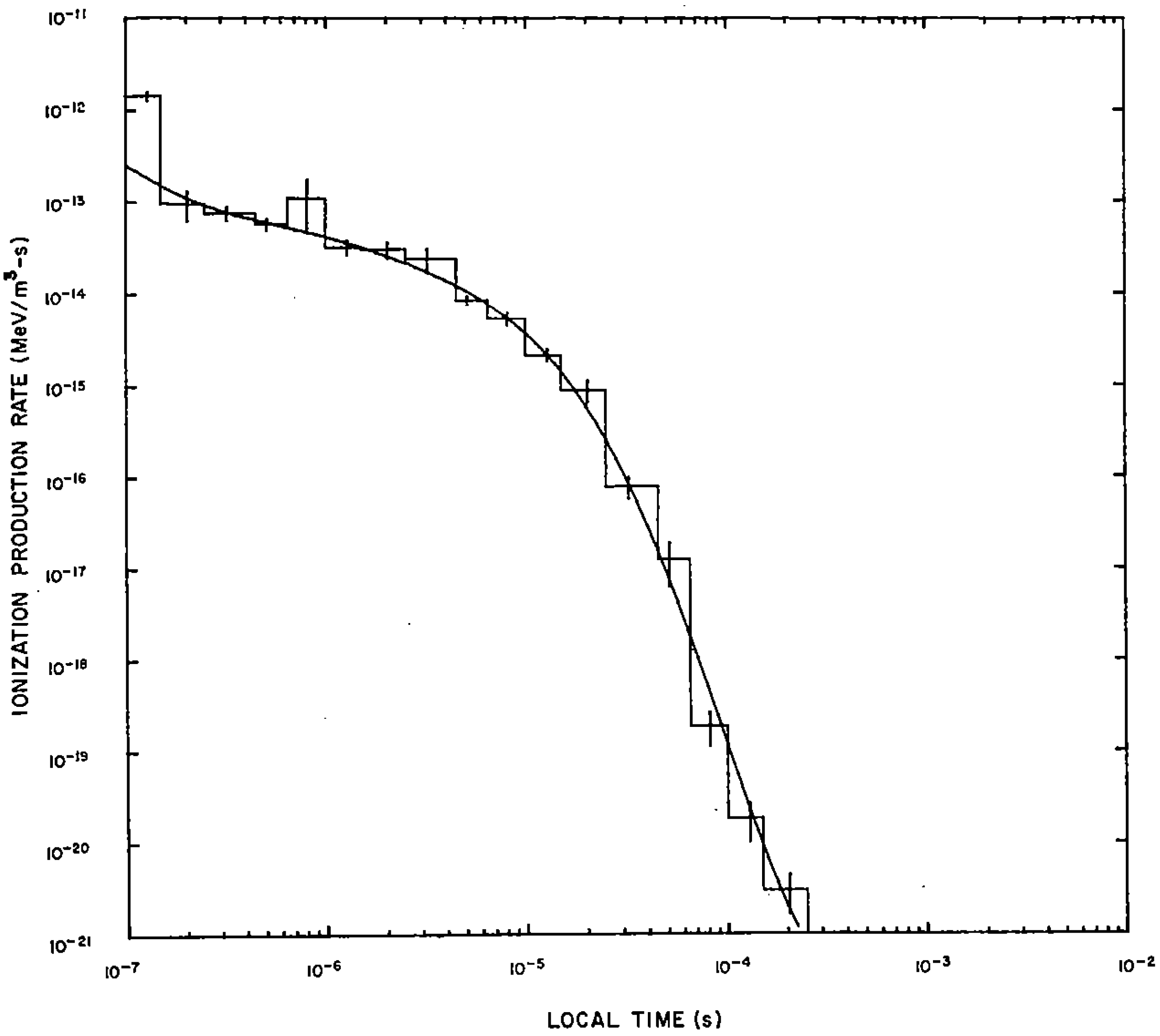

Figure 11. Ionization rate versus time for detector 10.

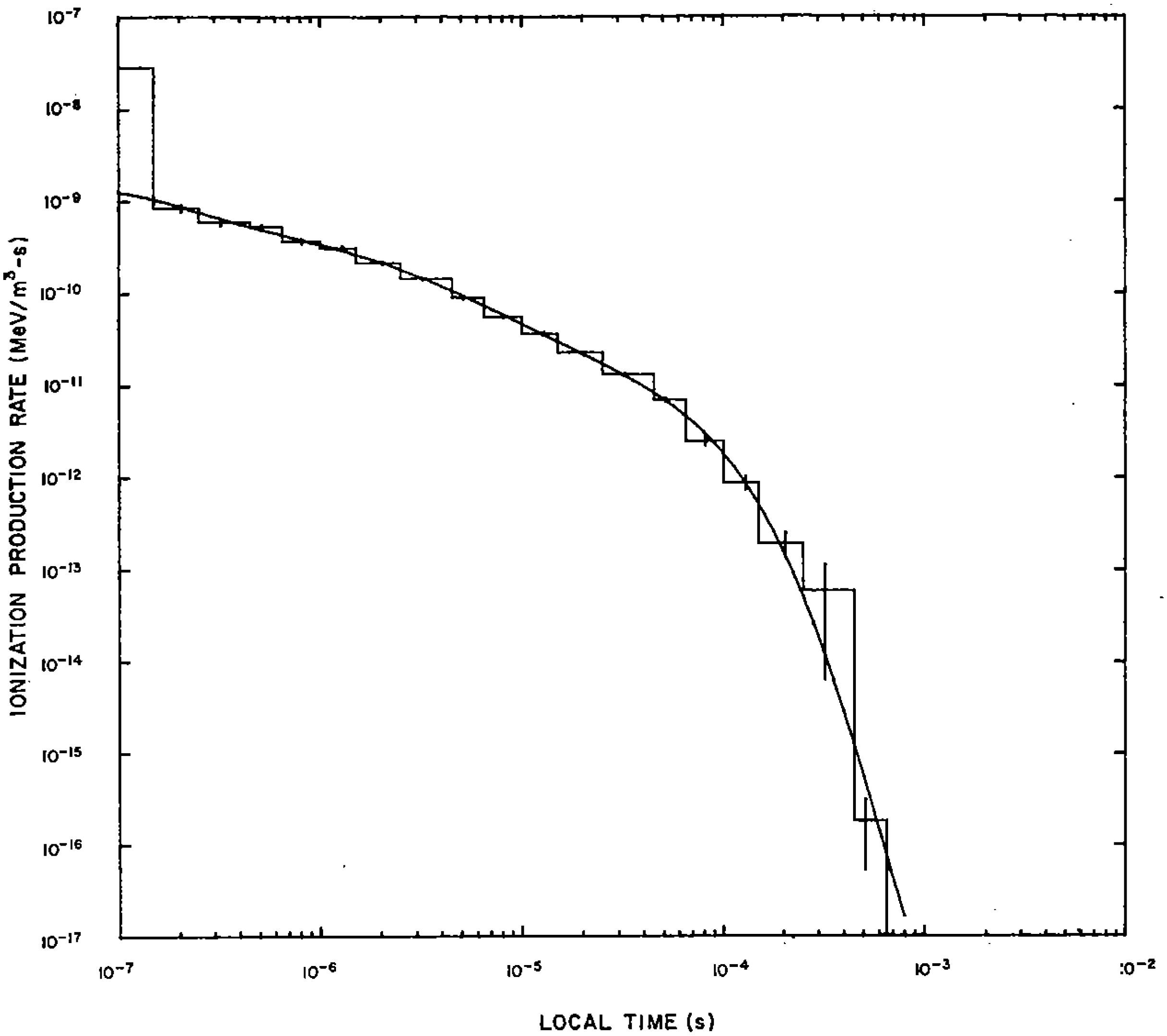

Figure 12. Ionization rate versus time for detector 11.

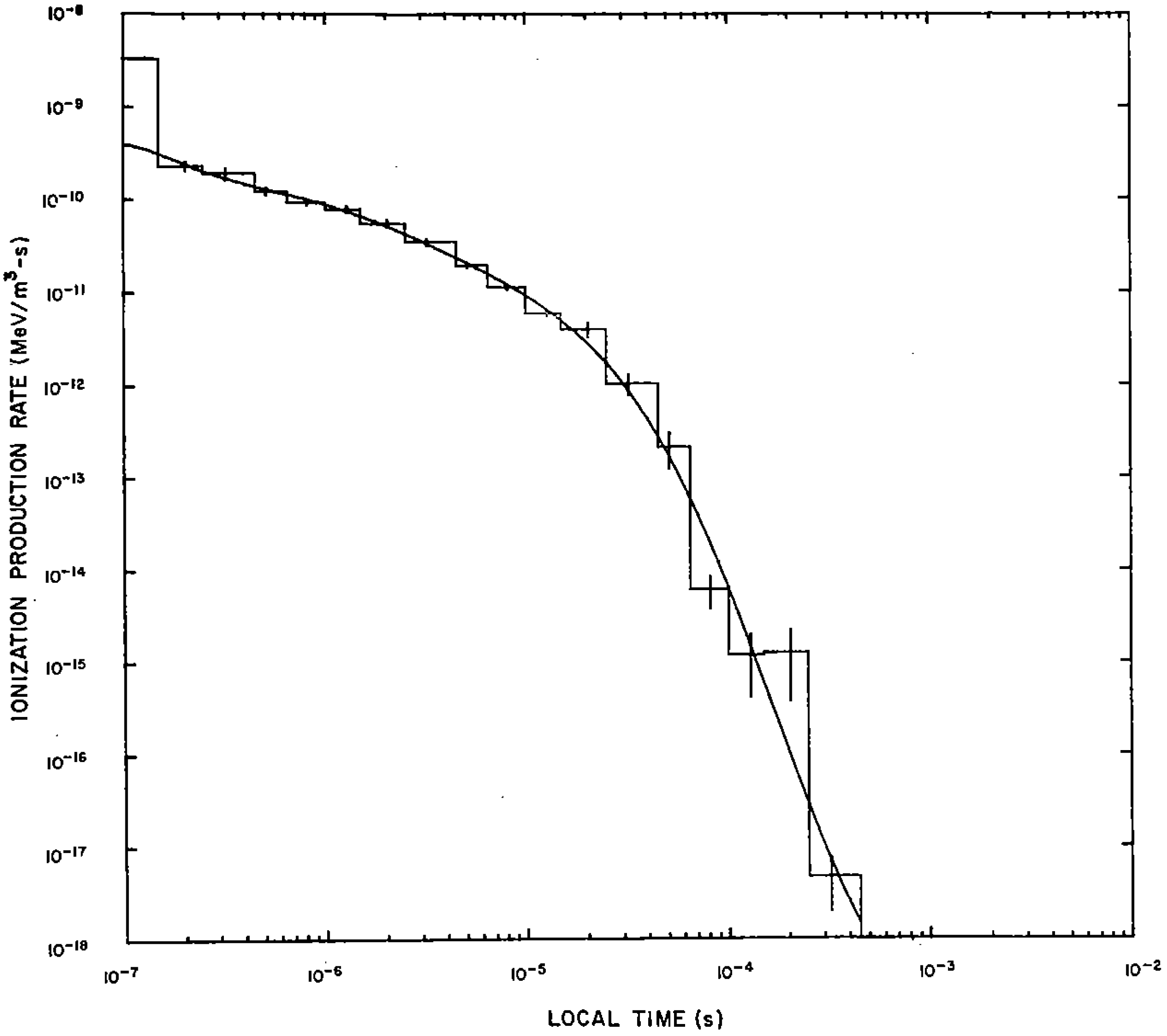

Figure 13. Ionization rate versus time for detector 12.

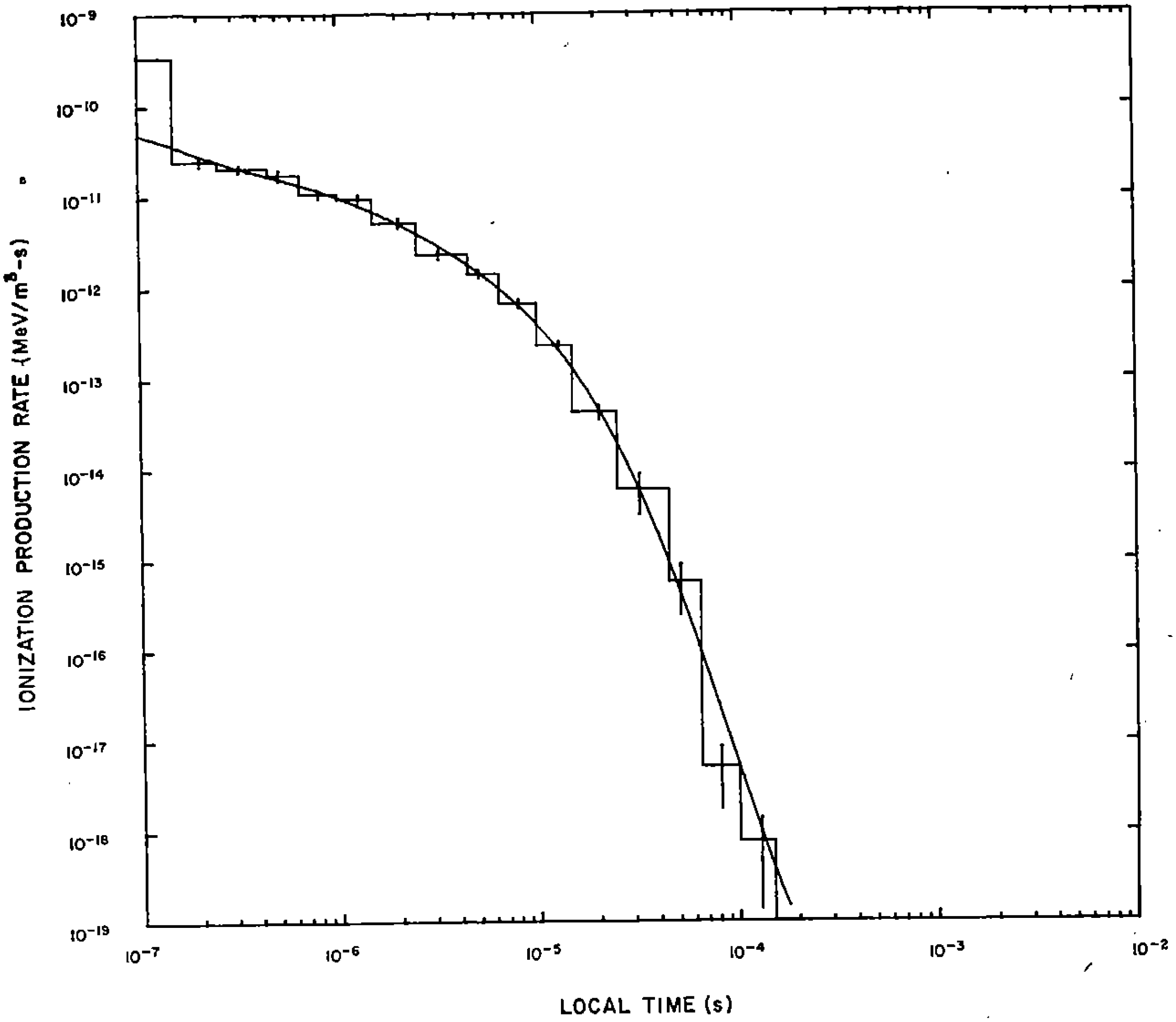

Figure 14. Ionization rate versus time for detector 13.

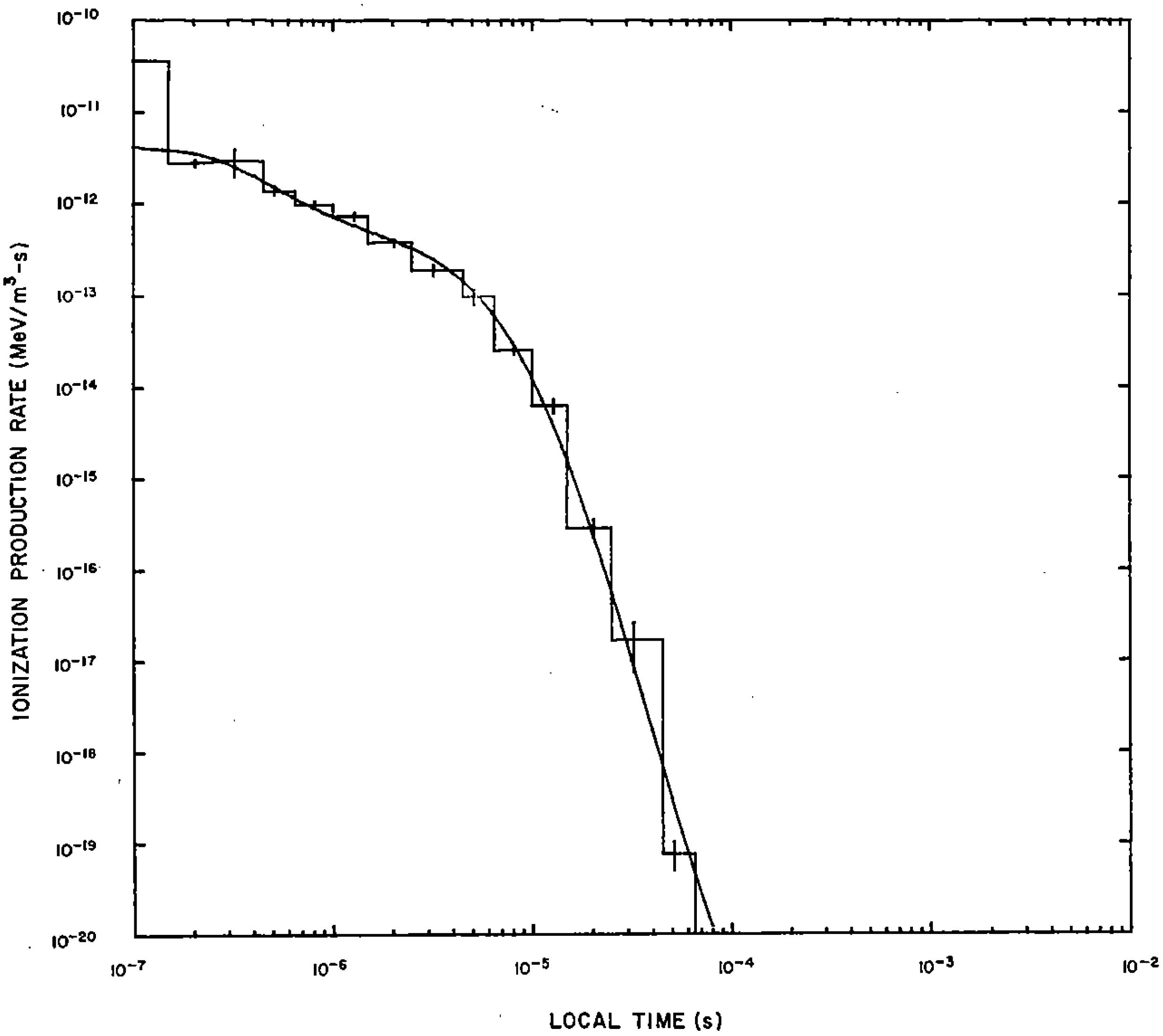

Figure 15. Ionization rate versus time for detector 14.

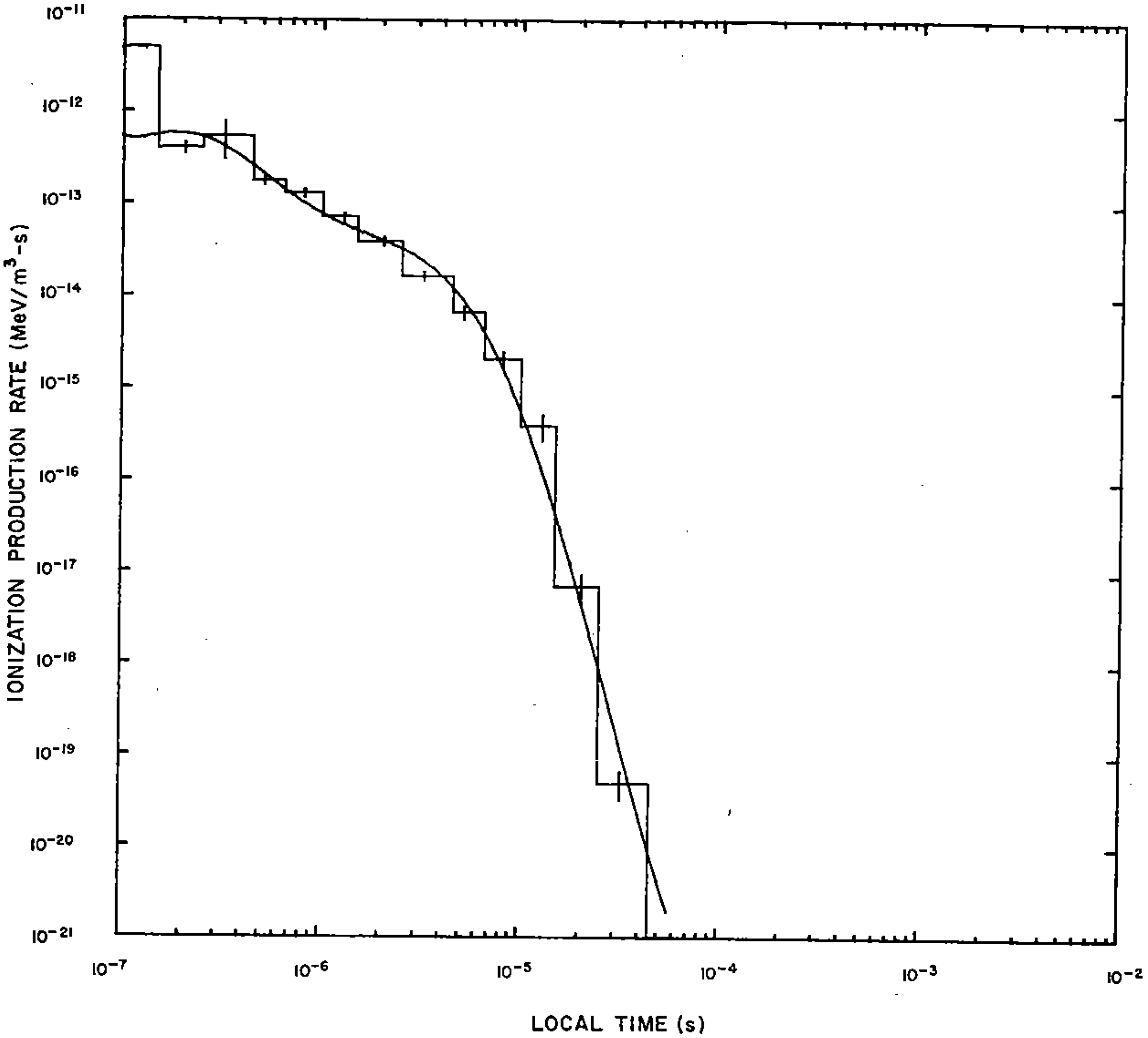

Figure 16. Ionization rate versus time for detector 15.

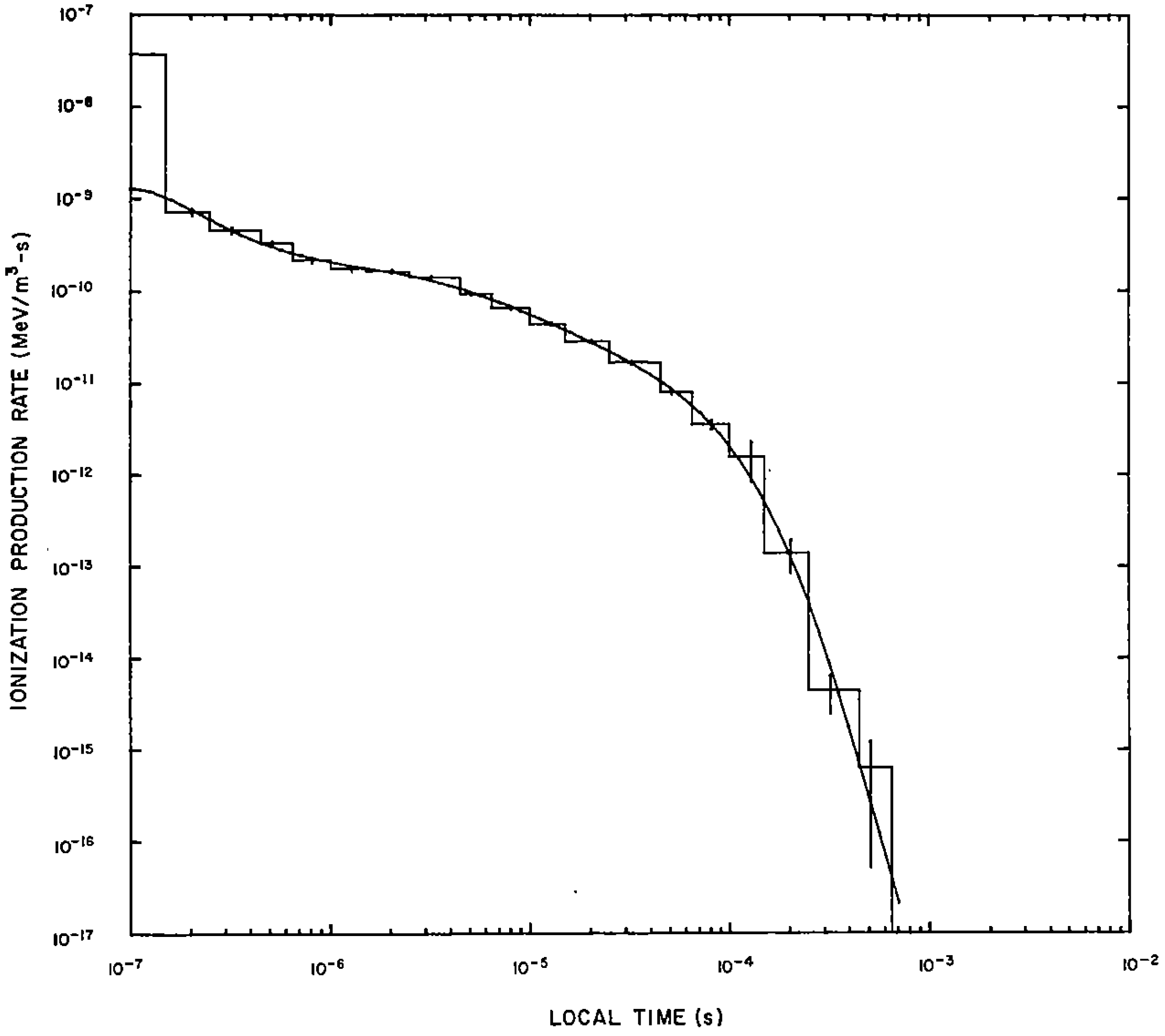

Figure 17. Ionization rate versus time for detector 16.

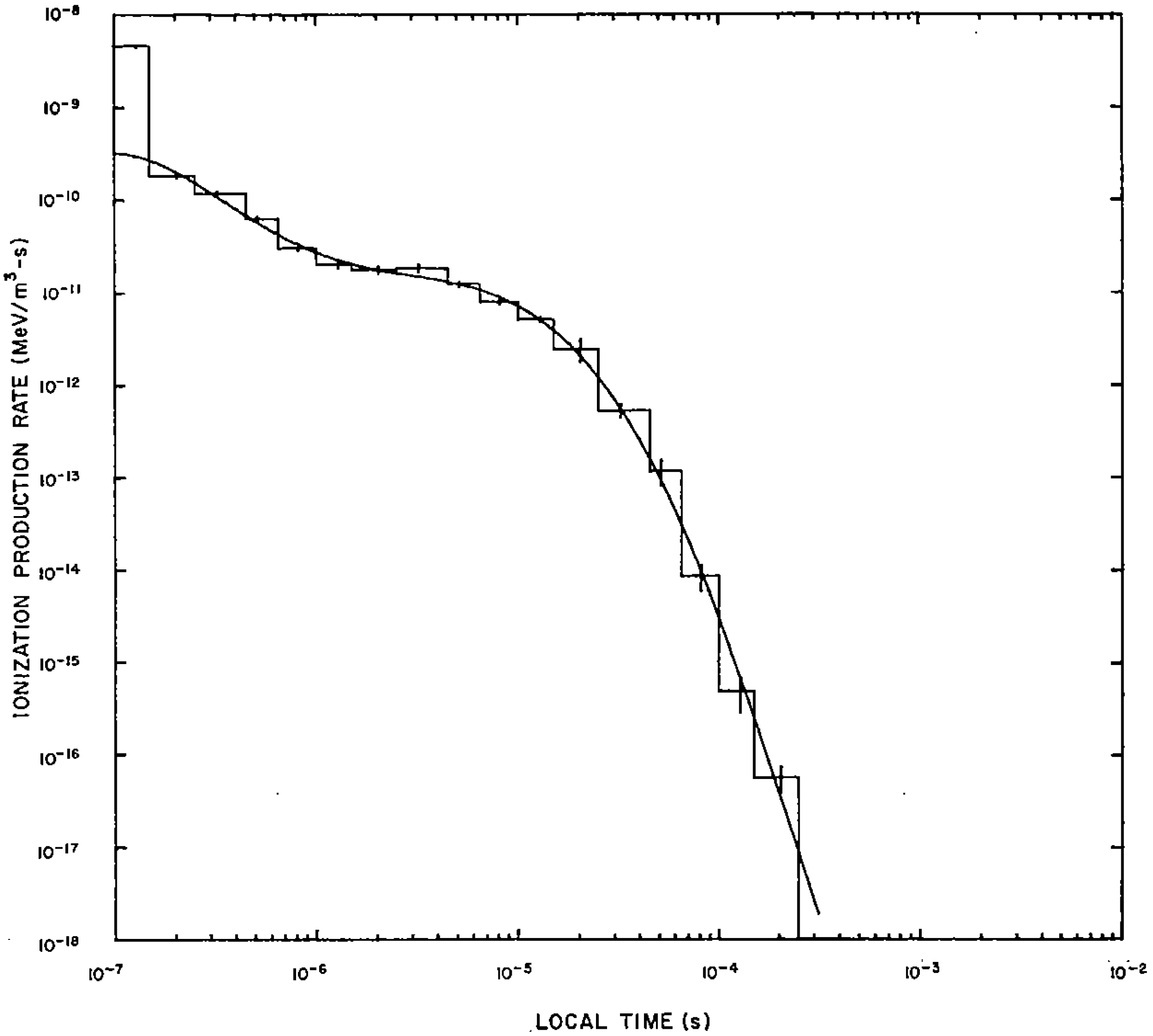

Figure 18. Ionization rate versus time for detector 17.

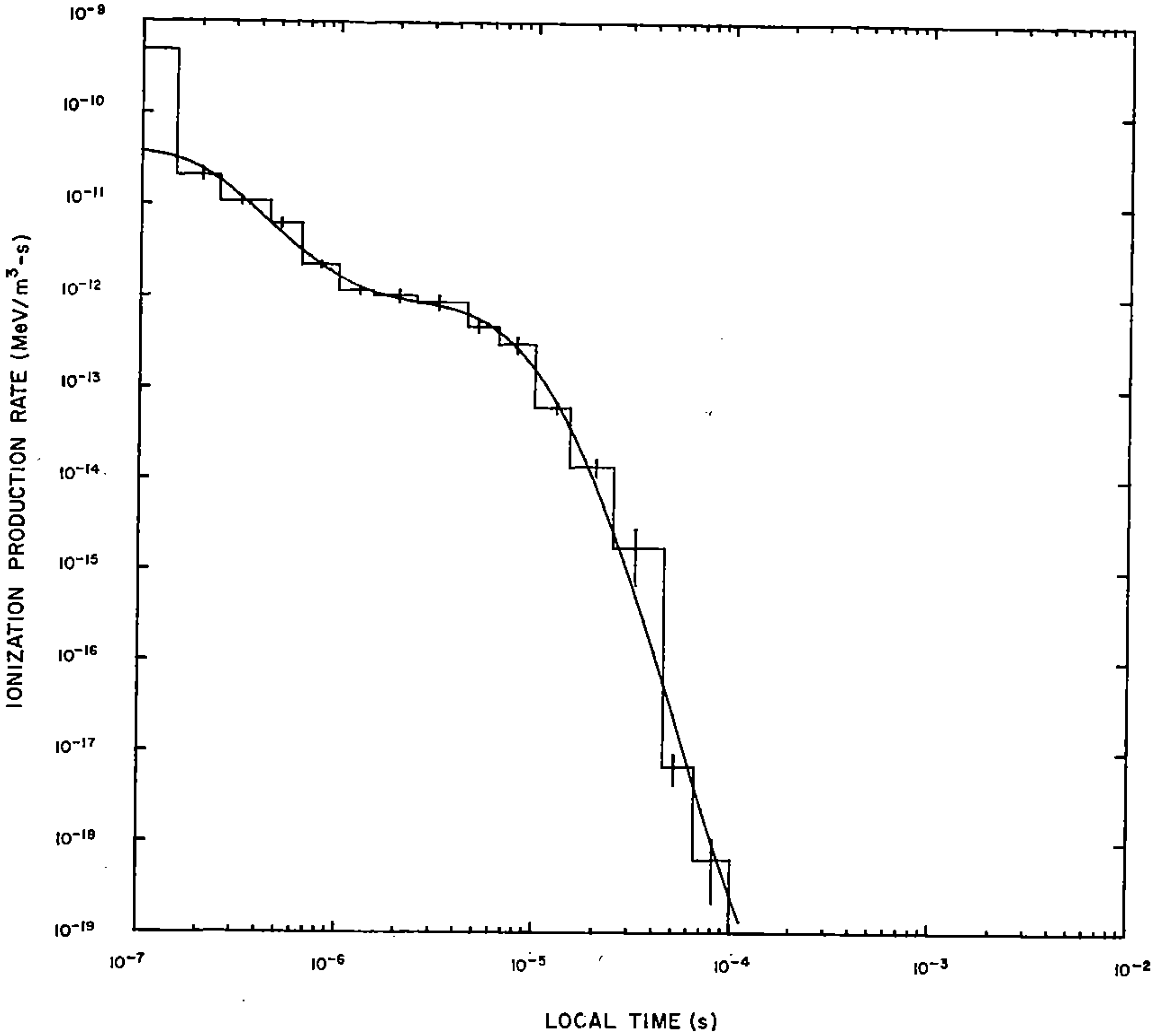

Figure 19. Ionization rate versus time for detector 18.

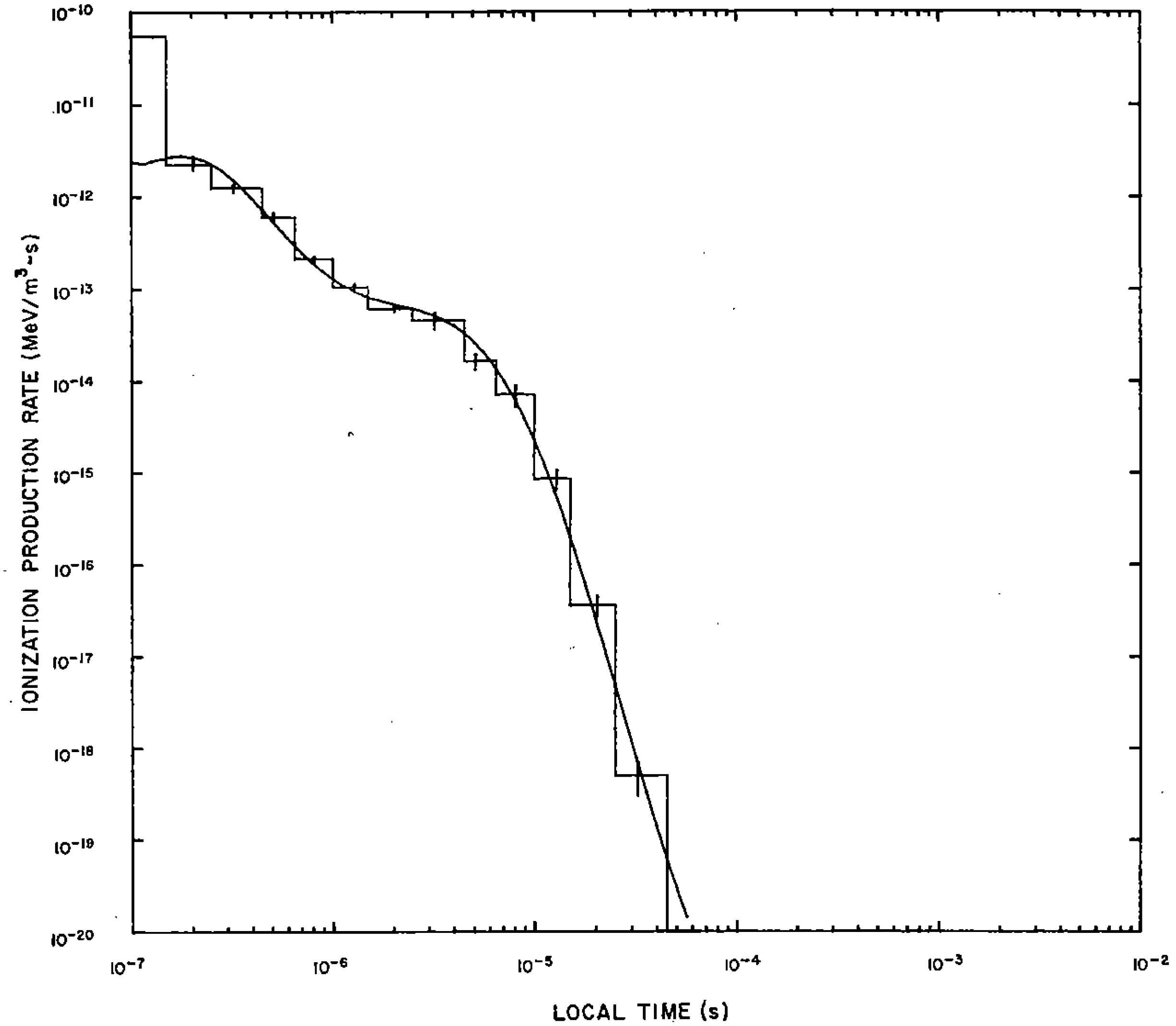

Figure 20. Ionization rate versus time for detector 19.

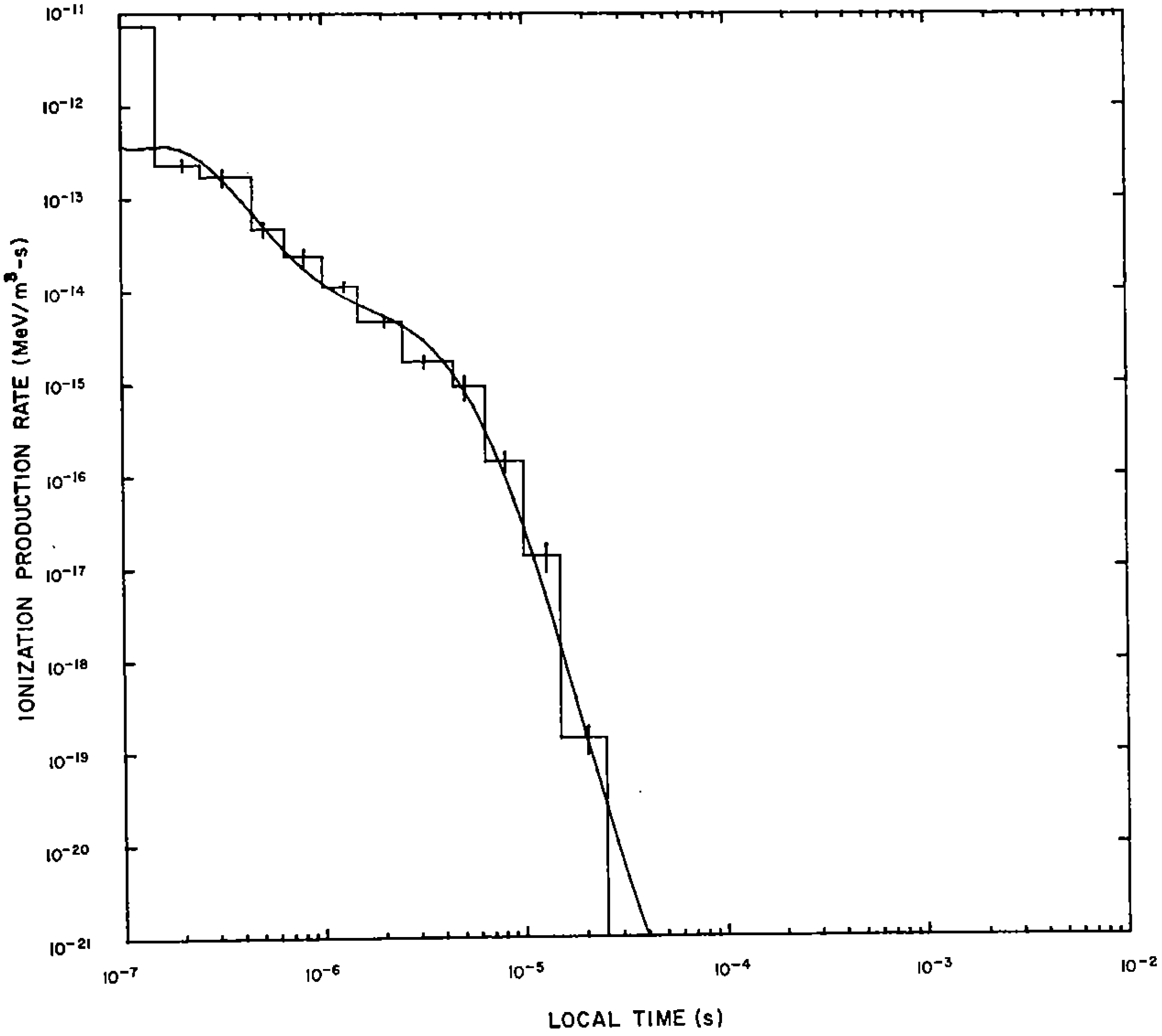

Figure 21. Ionization rate versus time for detector 20.

Detectors 1 to 5 denote those at 1, 5, 10, 15, and 20 neutron mfp's, respectively, along the radial 5 deg below the horizontal. Similarly, detectors 6 to 10 denote the ones along the 30-deg radial; 11 to 15, those along the 60-deg radial; and 16 to 20, those directly below the source. Each time bin has an associated standard deviation plotted as an error bar for each line. The absence of a lower bar (e.g., about 10^{-4} s in fig. 9) indicates a standard deviation ≥ 100 percent.

An eighth-order polynomial has been fitted to the data at each detector. Each bin has been weighted with the inverse square of its probable error. Appendix A details the calculation. The polynomial coefficients, a_i, for the fit

$$Y = \sum_{0}^{m} a_i X^i$$

are given in table I. The variable Y is the common logarithm of the ionization production rate; the variable X is $7 + \log_{10} t$, where t is local time in seconds.

TABLE I. POLYNOMIAL COEFFICIENTS

a_0	a_1	a_2	a_3	a_4	a_5	a_6	a_7	a_8
-10.9436	-0.361044	-0.483336	1.69238	-2.17473	1.38796	-0.492802	0.0927065	-0.00717815
-12.3223	-0.154085	-2.58666	4.65208	-3.61780	1.50766	-0.368348	0.0518322	-0.00335923
-13.5412	-0.480200	2.75848	-6.46288	6.75341	-3.66412	1.06615	-0.156692	0.00903135
-14.3964	-0.0170943	2.28469	-8.57783	11.1225	-6.85829	2.19354	-0.351484	0.0222237
-15.7378	-0.368802	9.83493	-25.2504	27.9594	-16.0098	4.96175	-0.790276	0.0505865
- 9.54119	-0.320991	-0.732876	1.09875	-0.427337	-0.272942	0.249978	-0.0655443	0.00570311
-10.1523	-0.447483	-1.01217	2.51621	-2.03569	0.433811	0.158126	-0.0798832	0.00895507
-11.1254	0.265371	-4.01799	7.36420	-6.18286	2.47639	-0.411331	0.000393750	0.00467776
-11.9903	0.0179967	-4.21753	9.25315	-9.40185	4.99227	-1.41630	0.197572	-0.0103209
-12.6025	-1.18708	-1.01026	5.57805	-8.07470	5.66324	-2.10947	0.392463	-0.0284886
- 8.90558	-0.173087	-1.76108	2.67788	-2.06110	0.571042	0.0125554	-0.0326621	0.00400831
- 9.41224	-0.0387803	-4.37073	10.3826	-11.6448	6.93472	-2.25149	0.372113	-0.0243915
-10.3186	-0.345842	-3.01639	8.40665	-10.6932	7.08266	-2.54384	0.461853	-0.0329663
-11.3781	-0.503988	3.14138	-10.9999	13.3154	-7.54260	2.07500	-0.261673	0.0114369
-12.2848	-0.642136	6.15582	-26.7103	33.1291	-20.1588	6.32650	-0.983141	0.0599368
- 8.88922	-0.0394376	-3.71197	5.35530	-2.88055	0.313617	0.251844	-0.0905675	0.00879928
- 9.49482	-0.00643099	-2.51443	0.901710	1.70321	-1.65210	0.596894	-0.103443	0.00729883
-10.4275	-0.348057	0.964514	-9.25196	13.1184	-7.73222	2.16949	-0.283459	0.0135223
-11.6253	-0.616258	10.0944	-36.0642	45.9322	-28.2471	8.97509	-1.41991	0.0886206
-12.4385	-0.769995	9.58638	-36.7599	49.6246	-32.3039	10.8413	-1.60721	0.118574

Additionally, a fourth-order fit was performed for these results, and the polynomial coefficients, b_i, for

$$Y = \sum_{0}^{m} b_i X^i$$

are given in table II. These reduced coefficients represent the data well, conserve space, and permit quick interpolation of results for positions between detectors. The interpolation technique developed is discussed in appendix B.

TABLE II. ECONOMIZED POLYNOMIAL COEFFICIENTS

Detector	Range	b_o	b_2	b_3	b_4
1	3.50	-11.0253	-0.292984	0.0462654	-0.00904505
2	3.50	-12.4583	-0.579686	0.314328	-0.0629281
3	3.70	-13.5355	-0.374246	0.253227	-0.0568493
4	3.75	-14.3666	-0.408617	0.355919	-0.0795904
5	3.80	-15.4952	-0.0544569	0.297131	-0.0889024
6	3.20	- 9.61626	-0.566180	0.209610	-0.0376100
7	3.00	-10.2465	-0.595884	0.253648	-0.0546639
8	2.85	-11.1720	-0.874045	0.513968	-0.119167
9	2.70	-12.0675	-1.11509	0.753022	-0.182827
10	2.45	-12.7692	-1.66227	1.36376	-0.367078
11	3.10	- 8.97439	-0.817716	0.389060	-0.0730703
12	2.65	- 9.49048	-1.22620	0.819261	-0.197043
13	2.35	-10.4013	-1.32988	0.960799	-0.271403
14	2.10	-11.3539	-1.79776	1.53173	-0.473854
15	2.05	-12.1941	-1.69806	1.31404	-0.415739
16	3.10	- 9.00820	-1.32099	0.839669	-0.167209
17	2.60	- 9.50877	-2.63144	2.06698	-0.475981
18	2.20	-10.3858	-3.66620	3.12280	-0.794678
19	2.00	-11.4810	-2.72896	1.97507	-0.484148
20	1.80	-12.3464	-2.95472	1.95235	-0.44342

3. DISCUSSION

To present important results that distinguish this study, two detector positions are compared. Subsequently, the results at the remaining detectors are discussed and related to a general pattern.

The selected results are for the fission gamma spectrum at two detector positions. Detector 18 is directly below the source at a distance corresponding to 10 mfp lengths for a 14-MeV neutron. Detector 8 is at the same mass distance from the source, but along a radial at 30 deg below the horizontal. Both detectors experience approximately the same total ionization from the uncollided gamma flux from the source. Yet the pulse shapes differ markedly (fig. 9, 19). The data printout includes spectrum as a function of number of scatters, and analysis reveals that detector 8 experiences an additional ionization due to multiple scattering of 1.5 times that from the direct pulse, whereas detector 18 shows only an increase of 25 percent due to multiple scattering.

By about 6×10^{-7} s local time, the ionization production rate at detector 18 has dropped an order of magnitude. This drop corresponds to a distance $d = 3 \times 10^8 \times 6 \times 10^{-7} = 1.8 \times 10^2$ m = 0.18 km. But detector 18 is 30 km from the source. Thus, the major contribution at detector 18 comes from photons that have travelled less than $0.18/30 = 0.6$ percent further than the source distance. By about 4.5×10^{-6} s local time, the rate at detector 8 has dropped an order of magnitude. This drop corresponds to $d = 3 \times 10^8 \times 4.5 \times 10^{-6} = 1.35 \times 10^3$ m = 1.35 km. Detector 8 is 53.2 km from the source, and the major contribution at this detector is from photons that have travelled approximately 2.5 percent further than the source distance.

Figure 22 shows the cumulative fractional ionization as a function of the number of scatters that a photon must undergo to contribute that fraction of ionization at each detector. At 18, the detector directly below the source, fully 90 percent of the total ionization is received from photons that have scattered only three times. At 8, the detector along the 30-deg radial, that percentage is not reached until photons that have scattered up to 10 times are scored.

Important results are observed because of the different scattering contributions to ionization at detectors 18 and 8. First, when the ionization rate has dropped to about 10 percent of its initial value, the pulse from a δ-function source of fission gamma has persisted for about 0.6 μs local time for detector 18, whereas that at detector 8 has persisted for about 4.5 μs. Second, analysis of the scattering data shows that over 9 percent of the ionization due to scattered photons at detector 8 was caused by energies below 100 keV. However, the

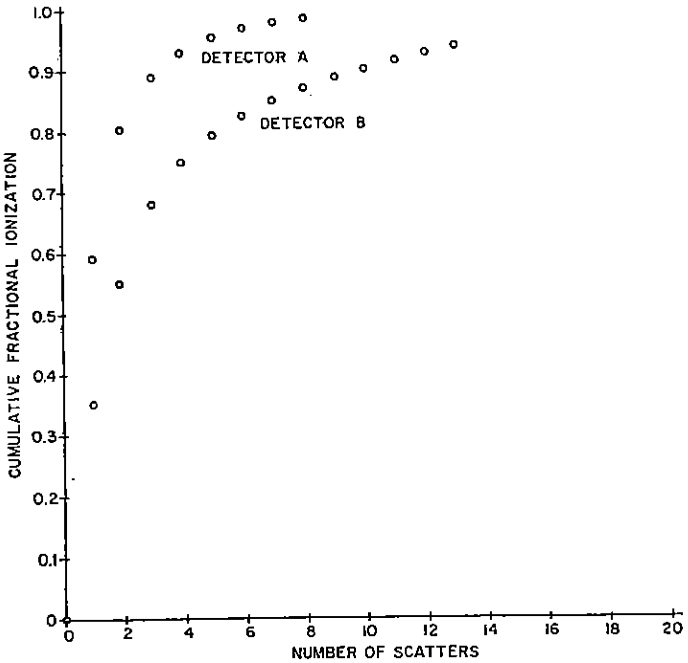

Figure 22. Ionization versus number of gamma photon scatters.

prolongation of the pulse is not primarily due to photons with energies below 100 keV, as can be seen in figure 23. The energy content of the pulses in the time range 1 to 1.5 ms can be compared after the pulse at detector 18 has ceased to be effective. The energy content of the pulse at detector 8 remains high.

This behavior can be seen also in figure 24, in which the photon flux in the energy range 1 to 1.5 MeV is plotted versus local time for detectors 8 and 18. These plots and those of the ionization rates in figures 9 and 19 are similar. Thus, higher energy photons continue to arrive at detector 8 at local time much later than at detector 18.

Part of this prolongation of the pulse in local time is due to the longer geometric distances traversed by the photons. Multiple scattering, however, appears to be a more important cause. An understanding of this subject can develop from the following simplistic analysis.

In figure 25, the source is at point A, detector 8 at point B, and detector 18 at point C. Forward scattering of the gamma ray is favored for Compton events. Consider all scattering points such that a scattering angle of ≤ 90 deg obtains between the source and the

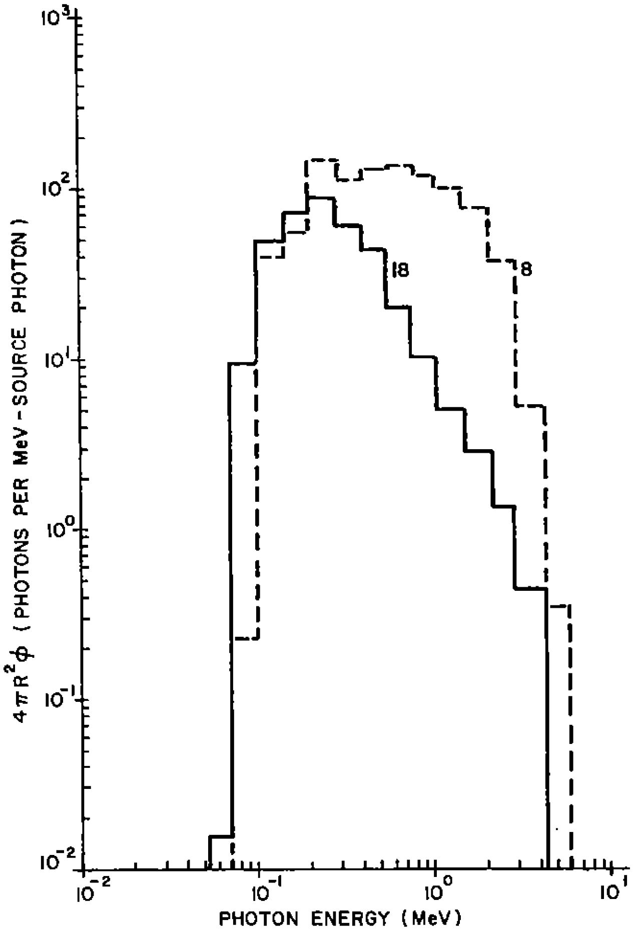

Figure 23. Energy-dependent flux plots for detectors 8 and 18 at local time 10^{-6} to 1.5×10^{-6} s.

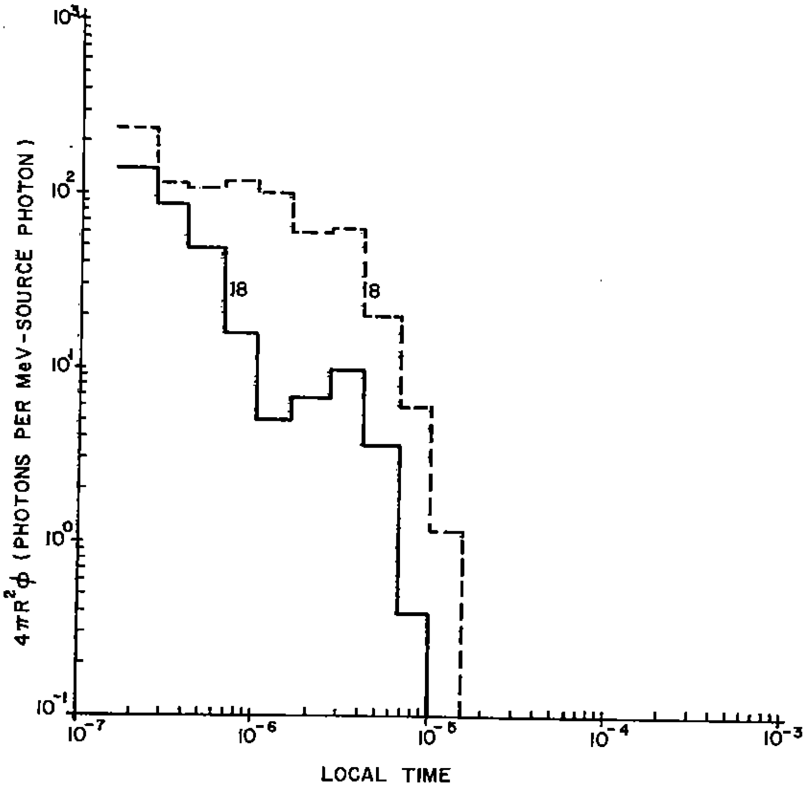

Figure 24. Time-dependent flux plots for detectors 8 and 18 at photon energy 1.1 to 1.5 MeV.

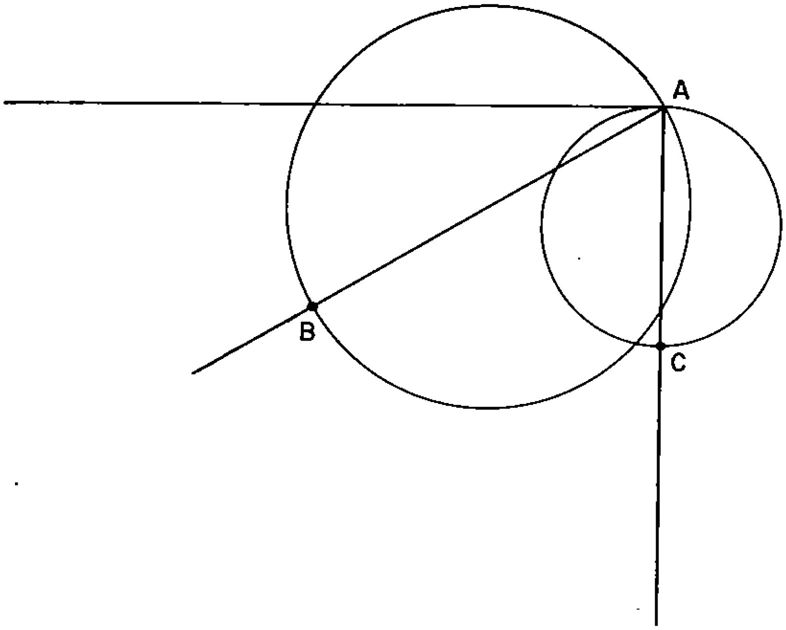

Figure 25. Geometrical relations for detectors 8 and 18.

detector. These points lie inside the sphere of diameter AC for detector 18 and AB for detector 8. Evidently, there are many more possible forward-scattering points toward detector 8 than toward detector 18. (For direct comparison of the number of points, the volume AC can be moved horizontally to the left until it is completely inside the volume AB, since the density variation is only in the vertical direction. All of the excess volume in AB contains possible forward-scattering points. Because of exponential density increase of the atmosphere, this is a considerable number in excess of that in AC.) Thus, forward scattering toward B is much more probable than toward C. Moreover, any photon that undergoes a second scattering in the large volume of AB not shared with AC already has its major component directed toward B. Only large-angle scattering could redirect it toward C.

Figure 26 helps one visualize the geometric effect of the changing density of the atmosphere with altitude. The source and detectors 8 and 18 are shown. The horizontal lines in arbitrary units represent the increasing density of the air as the altitude decreases.

Results for detectors 8 and 18 were compared in terms of ionization rate as a function of local time. The results obtained at the detector positions have been edited not for Compton source current, but for Compton source electrons produced (and tabulated by energy, angle, and time). The sheer volume of these results has precluded their presentation in this report. Examination of the tabulated gamma energy spectra and electron production results reveals that, for local times corresponding to those periods for which ionization rates are 10 to 100 times greater at detector 8 than at detector 18, the Compton source currents at detectors 8 and 18 differ also by the same magnitudes. The saturated field is given by the simple equation

$$E_{sat} = \frac{J_{comp}}{\sigma}$$

where E_{sat} is the saturated electric field strength, J_{comp} is the Compton source current, and σ is the atmospheric conductivity.

This field also is greater at detector 8 than at detector 18. (Conductivity σ varies only slightly, compared to J_{comp}.) These effects not only should be evident at the detector altitudes involved, but can be expected to have some influence in the near-surface region (W. T. Wyatt, private communication).

The results for detectors along the 30-deg radial from the source (fig. 6 to 10) are characterized by a broad pulse that slowly decreases in magnitude until late times. In the progression from detector 6 at

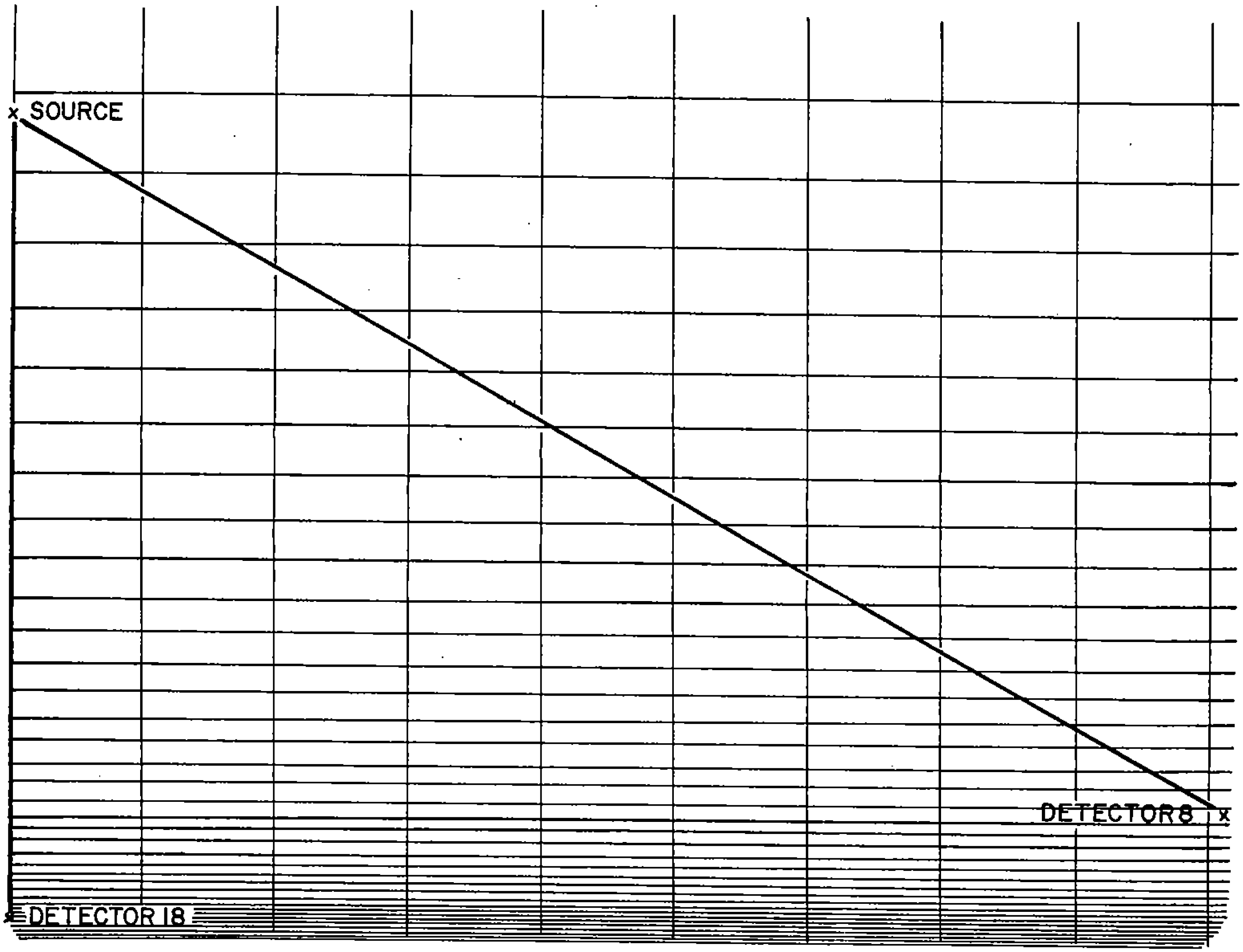

Figure 26. Source-detector geometries in density-dependent atmosphere.

1 14-MeV neutron mfp to detector 7 at 5 mfp, detector 8 at 10 mfp, detector 9 at 15 mfp, and detector 10 at 30 mfp, the magnitude and width of the pulses decreases.

When results for detectors along the 60-deg radial from the source are considered (fig. 12 to 16), initially the change as one progresses from 1 to 10 mfp is similar to that for the 30-deg radial. Pulse magnitude and width decrease. Pulse width decreases at a somewhat faster rate than aong the 30-deg radial. At 15 mfp, the pulse changes shape.

For these data, this change would not be easily seen without the polynomial fit of these results (fig. 15) and can be considered transitional. At 20 mfp, the transition in pulse shape has clearly taken place (fig. 16). The pulse shown like that at detector 18 (fig. 19) is characteristic of a large contribution to the total ionization by gamma photons that have scattered only a few times.

When results for detectors along the 90-deg radial from the source (i.e., directly below it) are considered (figs. 17 to 21), the changes in pulse shape are quickly apparent as one progresses from 1 to 20 mfp (fig. 17). At detector 18, the highly multiply scattered contribution has greatly decreased. The rate of falloff in pulse width from 1 to 20 mfp is faster along the 90-deg radial than along the 60-deg radial.

The rate of falloff in pulse width approaches its upper limit from detectors along the 30-deg radial to those at the 90-deg radial (directly below the source). Conversely, for the results for these detectors positioned along a 5-deg radial from the source (fig. 2 to 6), this rate of falloff approaches a lower limit. For these detectors, the contribution of multiply scattered gamma photons is so dominant that ionization rate pulses actually show peaks at very late times (0.01 to 0.1 ms) for detectors 4 and 5 (fig. 5, 6) and show almost no pulse width falloff in time from 1 to 20 mfp along the 5-deg radial.

4. CONCLUSIONS

For a primary gamma source at a 45-km height of burst, source-detector geometry importantly affects multiply scattered gamma photons in an atmosphere whose density depends on altitude. Significant changes in time and energy distributions of photon flux and in ionization rate have been recorded as a function of detector position in the atmosphere at constant source-detector mass distance. In addition, at altitudes where the exponential variation of the atmosphere is important, it is necessary to calculate transport to a low cutoff energy (10 keV), to adequately determine the ionization rate and total ionization. Finally, inclusion of these considerations in the calculations indicates that at late times for some source-detector geometries, the effect of Compton source current is much enhanced over other effects, since at these times the saturated field also is enhanced to approximately the same degree.

LITERATURE CITED

(1) T. M. Jordan, FASTER III, A Generalized Monte Carlo Computer Program for the Transport of Neutrons and Gamma Rays, vol. II, Users Manual, ART Research Corporation, ART-45 (November 1970).

(2) W. J. Veigele et al, X-Ray Cross Section Compilation from 0.1 keV to 1 MeV, Input Data and Supplemental Results, vol. II, Revision 1, Defense Nuclear Agency Report 2433F (31 July 1971).

(3) J. P. Roberts and J. S. Wicklund, Late-Time EMP Source Calculations at 45-km Height of Burst, Minutes of the EMP Phenomenology meeting at Science Applications, Inc., La Jolla, CA, 12-13 February 1974, Report SAI-74-211-LJ (25 March 1974), 83-86.

(4) J. P. Roberts and J. S. Wicklund, Gamma-Induced Ionization Rate Pulse Broadening in the Upper Atmosphere, ANS Transactions, 19 (October 1974), 441-442.

(5) W. E. Selph and M. B. Wells, Weapons Shielding Handbook (U), DASA 1892-4 (December 1969). (SECRET-RESTRICTED DATA)

(6) D. F. Higgins, C. L. Longmire, and A. A. O'Dell, A Method for Estimating the X-Ray Produced Electromagnetic Pulse Observed in the Source Region of a High-Altitude Burst (DNA-3218T), Mission Research Corporation (29 November 1973).

(7) J. P. Roberts and J. S. Wicklund, Transient Ionization Effects from Neutron-Secondary Gamma Radiation in the Upper Atmosphere, Harry Diamond Laboratories TR-1727 (October 1975).

(8) E. A. Straker, Status of Neutron Transport in the Atmosphere, ORNL-TM-3065 (29 July 1970).

APPENDIX A.--CURVE FITTING THE SCATTERED PRIMARY GAMMA RADIATION DATA

Histogrammic plots of the data and the associated standard deviation for each time bin are given in figures 2 to 21 in the body of the report. The few figures in which the error bars do not extend below the top line indicate that the associated error is 100 percent or greater. The first time bin contains the direct contribution and the amount due to scattering. In general, this bin should always be treated separately, since it includes the source history. The time for each detector is local time; i.e., the zero of time occurs at the arrival of the first photon at that detector.

The data were plotted on a log-log basis, with the understanding that the first time bin includes all contributions between 0 and 1.5×10^{-7} s. Then they were least-squares fitted on a log-log basis; i.e., the common logarithm of the dependent variable was least-squares fitted to an eighth-order polynomial in the common logarithm of the independent variable. Three purposes were behind the choice of an eighth-order equation: (1) to assure a strong drop-off at the end of the pulse, with no subsequent increase during the time interval of interest; (2) to provide enough degrees of freedom to detect small, but possibly significant, variations; and (3) to represent the data accurately enough for simplifications to be performed if warranted by the data. The direct contribution in the first time bin was ignored in the fitting.

The calculation proceeded as follows: Let the ionization production rate be given by y, and let t be the time in seconds. Set $Y = \log_{10} y$ and $X = 7 + \log_{10} t$ (this puts the zero of x at 10^{-7} s; in effect, it makes 0.1 μs the unit of time). We seek least-squares coefficients, a_i, such that

$$Y = \sum_{0}^{8} a_i X^i .$$

The transformations give a scale linear in X. The calculation of the least-squares coefficients can be greatly facilitated if equal increments of X can be taken. At first glance, it appears that this cannot be done here, since the intervals are 1 to 1.5, 1.5 to 2.5, 2.5 to 4, 4 to 6.5, and 6.5 to 10, repeating for several decades. Clearly, the midpoints of these intervals are not equispaced on a log scale, though their widths of 0.176, 0.222, 0.204, 0.211, and 0.187 per decade are not bad divisions.

It is possible to obtain equispaced points, each of which lies near the middle of each interval. The points must be spaced 0.2 of a decade apart for five intervals. One can select a starting value X_o, such that the sum of the squares of the distances of these equispaced points from the centers of their intervals is a minimum. That is, it is possible to select X_o such that

$$\sum\delta^2 = \left(X_o - \log 1.25\right)^2 + \left(X_o + 0.2 - \log 2\right)^2$$
$$+ \left(X_o + 0.4 - \log 3.25\right)^2 + \left(X_o + 0.6 - \log 5.25\right)^2$$
$$+ \left(X_o + 0.8 - \log 8.25\right)^2$$

is a minimum. Then

$$\partial\left(\Sigma\delta^2\right) / \partial X_o = 0$$

gives $X_o = 0.1093$. Corresponding values of time are 1.286, 2.038, 3.231, 5.120, and 8.115, which differ from the exact midpoints by 2.9, 1.9, 0.6, 2.5, and 1.6 percent. Thus, no significant degradation occurs by use of equispaced values of X.

Each data point in the least-squares fit was weighted by the inverse square of the standard deviation. The standard deviation has two sources: the variation in the dependent variable due to the statistical nature of the Monte Carlo data and the fact that the time bins have width. The former is usually the more important. It can be shown that if σ_A is the standard deviation associated with the quantity A, the standard deviation associated with its logarithm is given by $\sigma_{\log A} = \sigma_A/A$. The Monte Carlo calculation gives the standard deviation for the quantity in each time bin as a fraction of the mean value for that bin--i.e., it records

$$\delta_i = \frac{\sigma_i}{Y_i}\text{, so } \sigma_{Y_i} = \delta_i.$$

There is also a temporal error due to the width of the time bin. In the absence of a better guess, it can be assumed that the distribution is uniform over each bin. (Figures 2 to 21 in the body of the report indicate that this is generally true, except at the sharply dropping rear edge of the pulse. There, however, the uncertainty in Y so far overshadows the always-small uncertainty in X that the shape of the distribution across a bin is of no importance.) For a uniform distribution,

$$\sigma_j' = \frac{t_u - t_l}{\sqrt{12}}$$

where t_u and t_l are the upper and lower bounds, respectively, of the jth time bin. Thus,

$$\sigma_{X_j} = \frac{t_u - t_l}{\sqrt{12}\,\bar{t}}$$

where $\bar{t}$ is the mean value. Since the curve was fitted to the quantities $10^{X_o+0.2n}$, n = 0, 1, 2, . . . , and $X_o = 0.1093$, good estimates of each mean and bin width can be obtained by taking $\bar{t}_j = 10^{X_o+0.2n}$ as the mean, with bin edges $t_u = 10^{X_o+0.2n+0.1}$ and $t_l = 10^{X_o+0.2n-0.1}$.

Then

$$\sigma_{X_j} = \frac{1}{\sqrt{12}}\left(10^{0.1} - 10^{-0.1}\right) = \frac{0.4646}{\sqrt{12}} .$$

Under the reasonable assumption that the errors in Y arise from a different source than the errors in X, one can write

$$\sigma_j^2 = \sigma_{Y_i}^2 + \sigma_{X_i}^2$$

for the standard deviation for each data point. Finally, then, each point is weighted by the inverse square of its standard deviation, and the weighting factors are $W_i = \left[\delta_i^2 + 0.017988\right]^{-1}$. This formula supports the earlier contention that the exact distribution across each time bin is not very important, since δ_i is less than 0.1 only in those smooth regions where a uniform distribution is correct and rises sharply in the rapidly varying regions.

As is evident from figures 2 to 21, this fit is quite good; in general, it does about what one might expect, except in a few fits at very early times that have relatively large associated errors. In most fits, this size of error causes no problem, because the large source history is superimposed. In the body of the report, table I lists the coefficients, a_i, for the equation

$$Y = \sum_{0}^{8} a_i X^i$$

where $Y = \log_{10} Y$ and $X = \log_{10} t + 7$, $0 \leq X \leq 5$. In practice, the polynomial form is very useful, since, if written in the nested form $Y = a_0 + X \; (a_1 + X(a_2 + \; . \; . \; . \; + X(a_7 + Xa_8) \; . \; . \; .))$, it can be programmed into a two-step DO loop involving only eight additions and eight multiplications.

Study of table I and figures 2 to 21 soon convinces one that simplifications can be made. Several coefficients are not carrying their full weight: the curves appear to be smooth and of low order. Economizing the series appears possible without introducing much error.

One easy way to economize is to approximate the original series by one of lower order over a range. In general, a least-squares fit can be obtained through forming the quantity

$$Y = \sum_{0}^{n} a_i X^i - \sum_{0}^{m} b_i X^i, \quad m < n$$

and minimizing $\int_{R_o}^{R_1} Y^2 \, dX$ with respect to the various b's. If $R_o = 0$ and $R_1 = R$,

$$\frac{\partial}{\partial b_j} \int_{0}^{R} Y^2 \, dX = 2 \int_{0}^{R} Y \frac{\partial y}{\partial b_j} \, dX = - 2 \int_{0}^{R} \left(\sum_{0}^{n} a_i X^i - \sum_{0}^{m} b_i X^i \right) X^j \, dX = 0$$

at the minimum. Performing the integration, after factoring out a superfluous R,

$$\sum_{0}^{m} b_i \frac{R^{i+j}}{i + j + 1} = \sum_{0}^{n} \frac{a_i}{i + j + 1} R^{i+j}, \quad j = 0, 1, \; . \; . \; . \; m \; .$$

These provide m equations whose simultaneous solution gives the required least-squares b's.

Inspection of figures 2 to 21 indicates that probably no higher than fourth order is required to disclose the essential details. Moreover, the coefficient a_1 is usually so small that it might easily be zero. A zero slope at the origin for the approximating series would not introduce much error, would help remove the anomalies at very early times, and would provide an even simpler representation. Such considerations suggest a quartic representation with $b_1 = 0$.

The range is a subjective decision. In principle, it might be any value, but the fit in the region of interest becomes poorer as the range is increased. Accordingly, it was decided to approximate only over the range where the value of the ionization production rate is no less than 10^{-3} of a_o. The values for the range and the approximation coefficients for the fourth-order approximation are given in table II in the body of the report. The range is the number of decades; i.e., a range of 3.00 means that the approximation is valid in the region 10^{-7} to 10^{-4} s.

APPENDIX B.--INTERPOLATION OF THE SCATTERED PRIMARY RADIATION DATA

The coefficients in table II in the body of the report are "tighter" in that they do not vary as widely as those in table I in the body of the report. As a consequence, they admit of easier analysis than the coefficients of table I. Least-squares treatment of the coefficients b_o of table II as a function of 14-MeV neutron mean free paths (mfp's) along each line of detectors gives good agreement for both linear and exponential regressions. For the linear regression, the correlation coefficients are -0.992, -0.999, -0.999 and -0.997 for the angles 5, 30, 60, and 90 deg, respectively; the corresponding values for an exponential fit are 0.984, 0.997, 0.999, and 0.998. There seems to be little difference in choosing between them. The various coefficients are summarized in table B-I.

TABLE B-I. LEAST SQUARES FITS FOR ZEROTH ORDER COEFFICIENTS[1]

Declination angle (deg)	Least squares A + BX			Least squares A exp BX		
	A	B	Corr	A	B	Corr
5	-11.083	-0.22482	-0.992	-11.168	0.017256	0.984
30	- 9.4474	-0.16931	-0.999	- 9.5181	0.015203	0.997
60	- 8.7149	-0.17333	-0.999	-8.8015	0.016520	0.999
90	- 8.7029	-0.18070	-0.997	-8.7993	0.017088	0.998

[1] *Coefficients b_o as functions of 14-MeV neutron mean free paths.*

When the coefficients b_o are removed from the series of table II and the five residual series for each angle are plotted on the same graph, adjacent curves are sufficiently close to each other for simple interpolation (either linear or exponential) to be used. Thus, simple interpolation along any line of detectors would probably suffice, but the following scheme is not difficult and probably is less subject to error:

First, determine the distance to the point in question in terms of 14-MeV neutron mfp's. Call this n. Also, determine between which of the four tabulated angles of declination the point lies; call these angles θ_1 and θ_2. If linear interpolation is used, let n lie between the two tabulated mfp's n_1 and n_2. Let the pulse without b_o be given at n_1 by

$$\sum_{2}^{4} b_{i_1} x^{i}$$

and at n_2 by

$$\sum_2^4 b_{i_2} x^i .$$

The points n_1 and n_2 lie along the radial at angle θ_1. Then the pulse without b_o at n is given by

$$f \sum_2^4 b_{i_1} x^i + (1 - f) \sum_2^4 b_{i_2} x^i = \sum \left[f b_{i_1} + (1 - f) b_{i_2} \right] x_i$$

where

$$f = \frac{n_1 - n}{n_1 + n_2} .$$

Thus, determine the coefficients b_2', b_3', b_4' by simple interpolation: obtain b_0' through the appropriate equation from table B-I. Repeat the process for n mfp's at angle θ_2.

Points of equal mfp's are closely enough colinear so that linear interpolation is valid between two adjacent points. A simple geometric method can be used to obtain the pulse shape at the point in question. Let n_{θ_1} be at a physical distance of r_1 from the source, n_{θ_2} at a distance r_2 from the source, and n at a distance of r from the source. If the line between r_1 and r_2 is to be divided into x_1 and x_2 by r (or its extension), then

$$\left(x_1 + x_2\right)^2 = r_1^2 + r_2^2 - 2 r_1 r_2 \cos\left(\theta_1 - \theta_2\right)$$

and

$$x_1^2 = r_1^2 + r^2 - 2 r_1 r \cos \phi_1$$

where ϕ_1 is the angle between r_1 and r. From these two relations, obtain the factor $g = x_1/(x_1 + x_2)$ and get the final coefficients through

$$b_i = g b_{i\theta_1} + (1 - g) b_{i\theta_2} .$$

Because of the large distances involved, the atypical behavior, and the poorer correlation coefficient along the 5-deg declination line, interpolation in this region will probably be poorer than in those regions described by greater declination angles. (The region above 5 deg remains terra incognita.) In view of the fine correlation coefficients of table II, some extrapolation in distance is probably possible, especially along the larger angles of declination. However, the values in table II describe the situation adequately only until the scattered contribution drops to a thousandth of its initial value. After such time, the coefficients in table II are invalid, and an eighth-order polynomial with the coefficients of table I should be used (the same general interpolation scheme can be applied).